Nanoparticle and cell modifications using capillary electrophoresis

By

Mónica Filipa Neves Moço Alves

A dissertation submitted in fulfilment of the requirements for the Doctor of Philosophy

(Chemical Sciences)

School of Natural Sciences

University of Tasmania

May 2020

Declaration of Originality

I hereby declare that this thesis contains no material which has been accepted for a degree or diploma by the University or any other institution. To the best of my knowledge and belief, this thesis contains no material previously published or written by another person, except where due reference is made in the text of the thesis.

Monica Alves

22 May 2020

Authority of Access

This thesis may be made available for loan and limited copying and communication in accordance with the Copyright Act 1968.

Monica Alves

22 May 2020

Statement regarding published work contained in thesis

The publishers of the papers comprising Chapters 1 and 2 hold the copyright for that content, and access to the material should be sought from the respective journals. The remaining unpublished content of the thesis may be made available for loan and limited copying and communication in accordance with the Copyright Act 1968.

Monica Alves

22 May 2020

Acknowledgements

This PhD thesis required the input from many people to acquire some of the exciting results that we have achieved. Although the following words will never be enough to express all my appreciation to them, I would like to present here my gratitude for all their support for the past four years of my PhD.

I would like to thank my supervisor, Professor Michael Breadmore for giving me the opportunity to work on an innovative and exiting topic of my interest and be a member of his research group. I am extremely grateful for his never-ending enthusiastic, dedicated, and thoughtful scientific input during my PhD. I owe him immensely for his help, guidance, proof reading and scientific contributions in my manuscripts, oral and poster presentations as well as in this PhD thesis.

To my co-supervisor, Professor Mirek Macka, I will forever be grateful for believing in my abilities and bringing me to Tasmania to start my PhD, which was a truly life-changing experience for me. I have always been impressed by his wisdom in matters of science and beyond. Thank you for the guidance, mentorship, all the good conversations, and honest and friendly advices.

I am also very grateful to Professor Shane Powell, Professor Nuri Guven and Dr Ryan Nai for their crucial advices and insightful scientific discussions. To Professor Brett Paull and Professor Pavel Nesterenko, I would like to express my greatest appreciation for their valuable feedback and support during the first few months of my PhD. With their help, I successfully collected data that enabled my first PhD publication.

My sincere thanks to all staff within the Discipline of Chemistry and Australian Centre for Research on Separation Science (ACROSS) for their academic and technical support. In particular, I acknowledge Dr Petr Smejkal, Dr Sui Ching Phung, Dr Min Zhang, Dr Feng Li, Dr Yan Li and Dr Anton Peristyy for their kind help with the operation of analytical instrumentation.

A big thanks to all the members of my office, room 216, along with Atiyeah Ganjalinia and Brenda Mooney for all the great times, friendship, cheerful smiles, and sense of humour. I have every reason to convey my appreciation to each of you for the cooperation I have received.

I specially thank mom and dad for always believing that this could be possible! For their constant presence and unconditional support throughout the good and tough times. I would not have made it this far without them. To my dear brother, Nani, I express my thankfulness for being always an encourager and supporter in all the big steps I have taken.

Finally, I have no words to describe the gratitude and pride I have for my husband, Li. Thank you so much for all the love and care, support and understanding, even when it took some of our time. Thank you for making me a better person.

I dedicate my PhD degree to my little son Xavier, who was born only 9 hours after the acceptance of this thesis. He has made me stronger and more fulfilled than I could ever imagined. Xx

Statement of Co-authorship

The following people contributed to the publication of work undertaken as part of this thesis:

In Chapter 1, Paper 1: Alves, M. N., Miró, M., Breadmore, M. C., Macka, M. Trends in analytical separations of magnetic (nano) particles. *TrAC Trends in Analytical Chemistry* **2019**, 114, 89-97.

Monica Alves was the primary author and wrote the manuscript. Mirek Macka, Manuel Miró and Michael Breadmore contributed to the structure, formalisation and development of the manuscript. All co-authors assisted with refinement and presentation.

In Chapter 2, Paper 2: Alves, M. N., Nesterenko, P. N., Paull, B., Haddad, P. R., Macka, M. Separation of superparamagnetic magnetite nanoparticles by capillary zone electrophoresis using non-complexing and complexing electrolyte anions and tetramethylammonium as dispersing additive. *Electrophoresis* **2018**, 39, 1429-1436.

Monica Alves was the primary author and conducted all the experiments, analysed data and wrote the manuscript. Mirek Macka, Pavel Nesterenko, Brett Paull and Paul Haddad contributed to the idea, its formalisation and development. All co-authors assisted with refinement and presentation.

The following people contributed to the Australian Provisional Patent Application undertaken as part of this thesis:

In Chapter 6: M.N. Alves, M.C. Breadmore, Y.H. Nai, S. Powell, M. Macka, Isotachophoretic nucleic acid transformation of cells, Australian Provisional Patent Application No AU2019902240, Filed 26/6/2019.

Monica Alves was the primary creator (60% of contribution), conducted all the experiments and analysed the data. Michael Breadmore (15% of contribution) and Yi Heng Nai (15% of contribution) conceived the idea of the patent claims. Shane Powell (5% of contribution) and Mirek Macka (5% of contribution) assisted with the experimental design of the patent claims. Monica Alves, Michael Breadmore and Yi Heng Nai collaborate to write the claims and specifications of the invention through aggregate efforts. All creators assisted with the formalisation of the invention.

We the undersigned agree with the above stated "proportion of work undertaken" for each of the above published peer-reviewed manuscripts contributing to this thesis:

Signed:

Prof. Michael Breadmore	Prof. Simon Ellingsen
Supervisor	Head of School
School of Natural Sciences	School of Natural Sciences
University of Tasmania	University of Tasmania

Date: 29/1/2020

List of Publications

Journal articles

1. Alves, M. N., Miró, M., Breadmore, M. C., Macka, M. Trends in analytical separations of magnetic (nano) particles. *TrAC Trends in Analytical Chemistry* **2019**, 114, 89-97.

2. Alves, M. N., Nesterenko, P. N., Paull, B., Haddad, P. R., Macka, M. Separation of superparamagnetic magnetite nanoparticles by capillary zone electrophoresis using non-complexing and complexing electrolyte anions and tetramethylammonium as dispersing additive. *Electrophoresis* **2018**, 39, 1429-1436.

Patents

1. M.N. Alves, M.C. Breadmore, Y.H. Nai, S. Powell, M. Macka, Isotachophoretic nucleic acid transformation of cells, Australian Provisional Patent Application No AU2019902240, Filed 26/6/2019.

Conference presentations

1. Alves M. N., Nai Y. H., Powell S. M., Macka M., Breadmore M. C. Isotachophoresis for Rapid Transformation of *Escherichia coli*. In 2019 International Conference on Biotechnology and Bioengineering, Poznan, Poland, 2019 (oral).

2. Alves, M. N., Nesterenko, P. N., Paull, B., Macka, M. Separations and surface characterization of iron oxide nanoparticles by capillary electrophoresis. In RACI Research & Development Topics; Hobart, Australia, 2017 (poster).

3. Alves, M. N., Nesterenko, P. N., Paull, B., Macka, M. Separations and surface characterization of iron oxide nanoparticles by capillary electrophoresis. In AMN/ ISMN/ APCBM/ ANZNMF, Hobart, Australia, 2017 (poster).

4. Alves, M. N., Nesterenko, P. N., Paull, B., Macka, M. Separations and surface characterization of iron oxide nanoparticles by capillary electrophoresis. In RACI Research & Development Topics, Sydney, Australia, 2017 (poster).

5. Alves, M. N., Nesterenko, P. N., Paull, B., Macka, M. Separations and surface characterization of iron oxide magnetic nanoparticles by capillary electrophoresis**.** In ASASS 2 – ACROSS International Symposium on Advances in Separation Science; Hobart, Australia, 2016 (poster).

6. Alves, M. N., Nesterenko, P. N., Paull, B., Macka, M. Approaches to portable analysis of bioanalytes using micro- and paperfluidic platforms utilising enzymatic activities. In RACI Research & Development Topics, Melbourne, Australia, 2015 (poster).

Abstract

Particle separation and manipulation is a strength of electrophoresis. In this dissertation, firstly, the power of electrophoresis as a microanalytical technique is demonstrated by separations of bare magnetic nanoparticles provided for the first time electropherograms exhibiting symmetrical and highly reproducible peaks, free of spurious spikes characteristic of nanoparticle clusters. This was achieved using non-complexing (nitrate) and complexing (chloride, citrate and phosphate) electrolyte ions with additions of tetramethylammonium hydroxide. This enabled the separation of bare and functionalised magnetic nanoparticles. Secondly, CE was coupled to a magnetic field and trapping of magnetic nanoparticles was demonstrated using purposely selected electrolyte compositions.

Just like nanoparticles, cells exhibit an electric surface charge due to exposed charged or chargeable functional groups. Therefore, they migrate under the influence of an electric field. Through isotachophoretic focusing, the electrostatic adsorption of functionalised magnetic nanoparticles to the cell wall of *Escherichia coli* TOP10 and their cellular uptake was studied. The same strategy was applied for the ITP transformation of *E. coli* TOP10 with plasmid DNA. Counter pressure-assisted isotachophoresis brought a large excess of plasmid DNA in contact with the cell surface allowing for a transformation rate 1,000-fold higher compared to electroporation and chemical transfection at survival rates greater than 60%. Based on the findings, the ITP method was adjusted for effective transfection of mammalian cells (Jurkat T) showing similar robustness to electroporation. This opens possibilities of using the developed

method for the delivery of many other membrane impermeable solutes for screening of genes and drugs.

Table of Contents

Acknowledgements *i*

Statement of Co-authorship *iii*

List of Publications *vi*

Abstract *ix*

Table of Contents *xi*

List of Abbreviations *xv*

Preface *1*

Chapter 1. Trends in Analytical Separations of Magnetic (Nano) Particles *8*

Chapter 2. Separation of Superparamagnetic Magnetite Nanoparticles by Capillary Zone Electrophoresis using Non-complexing and Complexing Electrolyte Anions and Tetramethylammonium as Dispersing Additive *18*

Chapter 3. Online Magnetic Capture of Bare Superparamagnetic Magnetite Nanoparticles in a Capillary Electrophoresis System *30*

Abstract **30**

3.1 Introduction **30**

3.2 Experimental **31**

3.2.1 Reagents 31

3.2.2 Instrumentation 32

3.2.3 Capillary electrophoresis conditions 32

3.2.4 External permanent magnets and magnetic coil setup 32

3.3 Results and discussion 33

3.4 Conclusion 37

3.5 References 37

Chapter 4. Recent Developments in Capillary Electrophoresis of Prokaryotes and Eukaryotes *40*

Abstract 40

4.1 Introduction 40

4.2 Capillary electrophoresis of cells 42

4.2.1 Prokaryotes 42

4.2.2 Eukaryotes 46

4.3 Conclusion 48

4.4 References 49

Chapter 5. Isotachophoresis of Functionalised Magnetic Nanoparticles and Quantum Dots for Studies on Cell Uptake *54*

Abstract 54

5.1 Introduction 54

5.2 Experimental 55

5.2.1 Reagents 55

5.2.2 Capillary electrophoresis 56

5.2.3 Capillary conditioning 56

5.2.4 Electrolytes 56

5.2.5 Isotachophoresis 57

5.3 Results and discussion **57**

5.4 Conclusion **60**

5.5 References **61**

Chapter 6. Isotachophoresis for Rapid Transformation of Escherichia coli ***62***

Abstract **63**

Graphical Abstract **64**

6.1 Introduction **65**

6.2 Experimental **66**

6.2.1 Bacterial strain and preparation for ITP-based transformation. 66

6.2.2 Capillary electrophoresis. 66

6.2.3 Electrolytes 67

6.2.4 Capillary conditioning 67

6.2.5 ITP transformation 67

6.2.6 ITP transformation assisted with counter-pressure 68

6.2.7 ITP transformation success 68

6.2.8 Preparation of non-competent cells for chemical transformation and electroporation 68

6.3 Results and discussion **69**

6.4 Conclusion **75**

6.5 References **76**

Supplementary Information **78**

Chapter 7. Isotachophoresis and its Applicability to Transfection of Mammalian Cells ***81***

Abstract 81

7.1 Introduction 81

7.2 Experimental 82

7.2.1 Jurkat cells preparation 82

7.2.2 Capillary electrophoresis 83

7.2.3 Electrolytes 83

7.2.4 ITP transfection 83

7.2.5 ITP transfection success 84

7.2.6 Preparation of Jurkat cells for electroporation 84

7.3 Results and discussion 84

7.4 Conclusion 91

7.5 References 91

Chapter 8. Conclusions and future work ***93***

List of Abbreviations

AF4	Asymmetrical field flow fractionation
BGE	Background electrolyte
CE	Capillary electrophoresis
CFU	Colony-forming unit
CIEF	Capillary isoelectric focusing
CT	Chemical transformation
CZE	Capillary zone electrophoresis
DIC	Differential interference contrast
DLS	Dynamic light scattering
DLVO	Derjaguin-Landau-Verwey-Overbeek
DMSO	Dimethyl sulfoxide anhydrous
EP	Electroporation
FASI	Field amplified sample injection
FFF	Field flow fractionation
FISH	Fluorescence in situ hybridization
GFP	Green fluorescent protein
HEPES	4-(2-Hydroxyethyl)-1-piperazine ethanesulfonic acid
HGMS	High gradient magnetic separation
ICP-OES	Inductively coupled plasma-optical emission spectrometer
ITP	Isotachophoresis
LB	Luria-Bertani
LE	Leading electrolyte
LGMS	Low gradient magnetic separation

LOD	Limit of detection
LOQ	Limit of quantification
MALDI-TOF	Matrix assisted laser desorption ionization-time of flight
MALLS	Multi-angle laser light scattering
MEKC	Micellar electrokinetic chromatography
MNP	Magnetic nanoparticle
MRI	Magnetic resonance imaging
MRSA	Methicillin-resistant *Staphylococcus aureus*
MSSA	Methicillin-susceptible *Staphylococcus aureus*
PBS	Phosphate-buffered saline
PDDA	Poly (diallyldimethylammonium chloride)
PVP	Polyvinylpyrrolidone
RBC	Red blood cell
RSD	Relative standard deviation
SD	Standard deviation
SOC	Super optimal broth with catabolite repression
TE	Terminating electrolyte
TEM	Transmission electron microscopy
TMAOH	Tetramethylammonium hydroxide
TRIS	Tris(hydroxymethyl)aminomethane
UV	Ultraviolet
WBC	White blood cell

Preface

According to the diameter of particles, they can be classified into microparticles (1 to 1000 μm in size) and nanoparticles (1 to 100 nm in size). Particles having size between 100 and 1000 nm are commonly referred as submicron particles. Particles hold physical and chemical properties which are largely dependent on their size, specially below a certain threshold, due to so-called quantum effects. For example, nanoscale gold can appear red or purple at sizes inferior to 50 nm. The unique behaviour and increasing applications of micro- and nanoparticles have stimulated the advancement of new synthesis methods. Therefore, there is a large quantity of literature exploiting the synthesis and surface engineering of micro- and nanoparticles for many purposes. Considerably smaller reports have been done on approaches used for the analysis and separation of micro- and nanoparticles. Yet, it is critically important to obtain information on their size, shape, and surface chemistry to enable their practical use. Among the large range of micro- and nanoparticles, engineered magnetic nanoparticles (MNPs) made of iron and iron oxides are some of the most commonly used due to their biological compatibility, easy and low-cost of production, and high magnetic moment, allowing for their easy manipulation by an external field [1]. Chapter 1 of this dissertation discusses the integration of MNPs in analytical methods including field flow fractionation, capillary electrophoresis (CE), macroscale magnetophoresis and microchip magnetophoresis for the period between 2013 and 2018. Among these analytical methods, CE is the most powerful. Its advantages comprise the use of narrow capillaries with high electric resistance, allowing for the application of high electrical fields with minimal heat generation. The use of high electrical fields together with the conventional plug-type fluid flow from electrically driven systems results in

short analysis times and high efficiency and resolution for almost any type of ionic analytes. CE has found widespread use in a variety of subdisciplines for analysis of inorganic, organic, and biological species [2]. In the last 30 years, the realm of CE has been extended to the analysis of particles and cells.

In Chapter 2, separations of bare MNPs (ca. 11 nm) was performed using non-complexing and complexing electrolyte ions with additions of tetramethylammonium hydroxide (TMAOH), which is commonly applied to control the synthesis of stable iron oxides. The use of TMAOH as an electrolyte additive for CE separations provided for the first time electropherograms of bare MNPs exhibiting symmetrical and highly reproducible peaks, free of spurious spikes characteristic of nanoparticle clusters, allowing for the accurate determination of the electrophoretic mobility of bare MNPs. Using Tris-nitrate containing 20 mM of TMAOH as electrolyte, bare and carboxylated iron oxide nanoparticles were successfully separated.

Despite the well-known separation power of CE, one issue is its low sensitivity. Therefore, efficient online or offline sample preconcentration is usually required before separation. Magnetic solid phase extraction prior CE analysis using functionalised magnetic nanoparticles is gaining popularity due to its high extraction efficiency and convenience of operation. However, its implementation for online preconcentration in CE is limited. To develop insights on this topic, in Chapter 3, a method has been shown to capture MNPs in a CE system using external magnets. It was found that when 4 square NdFeB magnets are sequentially positioned within a capillary zone, and MNPs flow by pressure, ca. 68% of them are captured, corresponding to 20% higher capture than electrically driven MNPs.

Just like nanoparticles, in aqueous buffer solutions, cells exhibit an electric surface charge due to exposed charged or chargeable functional groups. Therefore, they migrate under the influence of an electric field. Chapter 4 discusses advances in CE, including isotachophoresis (ITP) and other CE modes, of prokaryotic and eukaryotic cells for the last 8 years. ITP is a robust electrokinetic stacking technique that can attain million-fold preconcentration and efficient separation based on ionic mobility. Recent studies have shown that ITP also have wider applications, namely, to enhance hybridization rate of complementary nucleic acid [3-8] and antibody-antigen interactions [9-11]. Moreover, Phung *et al*. utilized ITP to accelerate the intracellular transport of oligonucleotides into intact bacterial cells for in-line fluorescence in vitro hybridization (FISH) [12].

It has been demonstrated that highly charged electrostatic interactions between nanoparticles can induce membrane adsorption and intracellular uptake. To investigate the ITP effect in the electrostatic adsorption of MNPs to the cell wall and their intracellular uptake, in Chapter 5, carboxylic acid functionalized iron oxide nanoparticles (ca. 10 nm) were focused with *Escherichia coli* TOP10 cells at the same isotachophoretic boundary. After each ITP run, *E. coli* TOP10 cells from the outlet vial were incubated in rich medium and collected/washed with the help of an external magnet (see section 5.3). The cells incorporating or adsorbing magnetic nanoparticles in their membrane were determined by plate counting (see section 5.3). To increase the sensitivity of this method and reduce the assay time (ca. 16 hours). ITP focusing of QD-COOH (ca. 10 nm) and *E. coli* TOP10 cells was performed. After each ITP run, *E. coli* TOP10 cells from the outlet vial were incubated in rich medium and collected/washed by means of centrifugation and directly visualised by fluorescence

microscopy. Therefore, the overnight incubation step was eliminated. Due to the non-specificity of the labelling method described in Chapter 5, it can be applicable to every kind of cell in a rapid and simple way. The results obtained in Chapter 5 were promising; however, the sensitivity achieved was below expectations, thus, more powerful detection instrumentation will be used in further studies.

In Chapter 6, a similar strategy was used for the transformation of a small number of non-competent *Escherichia coli* TOP10 cells (2–3 x 10^5) at room temperature. Cells and plasmid DNA were sequentially injected into a 50 µm ID capillary and ITP-focused into 11.5 nL induced by application of high DC voltage (16 kV). Through ITP, a large excess of plasmid DNA was brought in contact with the cell surface (ratio of 114,974:1 *vs.* 2:1 in conventional chemical transformation and electroporation), with the contact time adjusted by application of a counter-pressure (1.3 psi) opposing the ITP movement. The transformation rate was more than 1,000-fold higher compared to electroporation and chemical transformation at survival rates greater than 60%. Several plasmids of up to 10 kb were successfully introduced into the *E. coli* TOP10 cells using the ITP-based transformation with counter-pressure (1.3 psi) for 21 minutes. This opens possibilities of using the developed method for the delivery of DNA plasmid into a wide range of cells types, including difficult to transfect cell lines.

Jurkat cells are an immortalised line of human T lymphocyte cells which has most often been used as a prototypical T cell line to study acute T cell leukemia, T cell signalling and the expression of various chemokine receptors susceptible to viral entry, particularly HIV. One important limitation of studying Jurkat cells is their inherent difficulty of being transfected offering frequencies which are sometimes insufficient for their use. In Chapter 7, the feasibility of using ITP to introduce plasmid DNA into

Jurkat cells was made by sequentially injecting plasmid DNA encoding for GFP and Jurkat cells into a Rtx wax (fused silica) capillary with 60 cm total length and 100 μm ID. Plasmid DNA and Jurkat cells were focused into 19 nL by ITP induced by application of constant voltage (3 kV). The expression of GFP was an indicator of transfection efficiency. Through this method, Jurkat cells were transfected at a rate of 88% with the vector pCMV6-AC-GFP, while EP of 10^6 and 10^3 cells only achieved 54% and 51%, respectively. The fact that both procedures involve the physical interaction between an electric field and the cell membrane, make them less dependent on cell type than other methods. However, ITP transfection is suitable for handling large sample sets when organized in 96-well plates adapted to a multichannel capillary electrophoresis device, which increases automation and sample processing throughput. The success of ITP transfection encourages the application of this method as a newly emerging attractive option for recombinant protein production and may be applicable to cell delivery of many other membrane impermeable solutes for screening of genes and drugs.

References

1. Beveridge, J. S.; Stephens, J. R.; Williams, M. E., The use of magnetic nanoparticles in analytical chemistry. *Annual Review of Analytical Chemistry* **2011,** *4*, 251.

2. Landers, J. P., *Handbook of capillary electrophoresis*. CRC press: 1996.

3. Persat, A.; Santiago, J. G., MicroRNA profiling by simultaneous selective isotachophoresis and hybridization with molecular beacons. *Anal. Chem.* **2011,** *83* (6), 2310.

4. Bercovici, M.; Kaigala, G.; Mach, K.; Han, C.; Liao, J.; Santiago, J., Rapid detection of urinary tract infections using isotachophoresis and molecular beacons. *Anal. Chem.* **2011,** *83* (11), 4110.

5. Lantz, A. W.; Brehm‐Stecher, B. F.; Armstrong, D. W., Combined capillary electrophoresis and DNA‐fluorescence in situ hybridization for rapid molecular identification of Salmonella Typhimurium in mixed culture. *Electrophoresis* **2008,** *29* (12), 2477.

6. Bercovici, M.; Han, C. M.; Liao, J. C.; Santiago, J. G., Rapid hybridization of nucleic acids using isotachophoresis. *Proc. Natl Acad. Sci. U.S.A* **2012,** *109* (28), 11127.

7. Bahga, S. S.; Han, C. M.; Santiago, J. G., Integration of rapid DNA hybridization and capillary zone electrophoresis using bidirectional isotachophoresis. *Analyst* **2013,** *138* (1), 87.

8. Eid, C.; Garcia-Schwarz, G.; Santiago, J. G., Isotachophoresis with ionic spacer and two-stage separation for high sensitivity DNA hybridization assay. *Analyst* **2013,** *138* (11), 3117.

9. Kawabata, T.; Wada, H. G.; Watanabe, M.; Satomura, S., "Electrokinetic Analyte Transport Assay" for α‐fetoprotein immunoassay integrates mixing, reaction and separation on‐chip. *Electrophoresis* **2008,** *29* (7), 1399.

10. Khnouf, R.; Goet, G.; Baier, T.; Hardt, S., Increasing the sensitivity of microfluidics based immunoassays using isotachophoresis. *Analyst* **2014,** *139* (18), 4564.

11. Paratore, F.; Zeidman Kalman, T.; Rosenfeld, T.; Kaigala, G. V.; Bercovici, M., Isotachophoresis-Based Surface Immunoassay. *Anal. Chem.* **2017,** *89*, 7373.

12. Phung, S. C.; Cabot, J. M.; Macka, M.; Powell, S. M.; Guijt, R. M.; Breadmore, M. C., Isotachophoretic Fluorescence in situ Hybridization of intact bacterial cells. *Anal. Chem.* **2017,** *89*, 6513.

Chapter 1. Trends in Analytical Separations of Magnetic (Nano) Particles

*The research contained in this chapter has been published as Alves, M. N., Miró, M., Breadmore, M. C., Macka, M. Trends in analytical separations of magnetic (nano) particles. *TrAC Trends in Analytical Chemistry* **2019**, 114, 89-97.

Trends in Analytical Chemistry 114 (2019) 89–97

Contents lists available at ScienceDirect

Trends in Analytical Chemistry

journal homepage: www.elsevier.com/locate/trac

Trends in analytical separations of magnetic (nano)particles

Mónica N. Alves [a], Manuel Miró [b], Michael C. Breadmore [a], Mirek Macka [a, c, d, *]

[a] School of Natural Sciences and Australian Centre for Research on Separation Science (ACROSS), University of Tasmania, Hobart, 7001, Australia
[b] FI-TRACE Group, Department of Chemistry, University of the Balearic Islands, Carretera de Valldemossa, km. 7.5, E-07122, Palma de Mallorca, Spain
[c] Department of Chemistry and Biochemistry, Mendel University in Brno, Zemedelska 1, 613 00, Brno, Czech Republic
[d] Central European Institute of Technology, Brno University of Technology, Purkynova 123, 612 00, Brno, Czech Republic

ARTICLE INFO

Article history:
Available online 2 March 2019

Keywords:
Capillary electrophoresis
Field flow fractionation
Magnetic (nano)particles
Magnetophoresis
Microfluidic chip
Separation

ABSTRACT

Magnetic particles (MPs) and magnetic nanoparticles (MNPs) are appealing candidates for biomedical and analytical applications due to their unique physical and chemical properties. Given that magnetic fields can be readily used to control the motion and properties of M(N)Ps, their integration in analytical methods opens new avenues for sensing and quantitative analysis. There is a large body of literature related to their synthesis, with a relatively small number of methods reporting the analysis of M(N)Ps using separation methods, which provide information on their purity and monodispersity. This review discusses analytical separation methods of M(N)Ps published between 2013 and June 2018. The analytical separation methods evaluated in this work include (i) field flow fractionation, (ii) capillary electrophoresis, (iii) macroscale magnetophoresis and (iv) microchip magnetophoresis. Among the trends in analytical separations of M(N)Ps an inclination towards miniaturization is moving from conventional benchtop methods to rapid and low-cost methods based on microfluidic devices.

1. Introduction

Magnetic (nano)particles (M(N)Ps) offer the unique advantage of being manipulated (moved or held in place) using permanent magnets or electromagnets, a significant reason behind their popularity, which grew rapidly in the past decades [1–3]. As an example, one of the most routinely used methods exploiting MPs is magnetic sorting of cell populations from biological suspensions [4]. This method is now standardized for tissue engineering and medical analysis.

Magnetic nanoparticles (MNPs) exhibit physical properties that differ remarkably from those of the bulk ferromagnetic material due to finite size effects such as high surface-to-volume ratio, and a special magnetic property at diameters typically lower than 20 nm called superparamagnetism [5]. At such small size, MNPs do not exhibit multiple magnetic domains like ferromagnetic particles, but instead a single domain. Therefore, under an external magnetic field, the magnetic moment of single domain nanoparticles quickly aligns with the applied field, but in its absence, they exhibit no net magnetisation due to the rapid reversal of their magnetic moment. It makes superparamagnetic nanoparticles especially suitable when looking for fast responses to external magnetic fields without agglomeration effects [6]. For this reason, superparamagnetic nanoparticles have been extensively pursued for a vast variety of biomedical applications, including biosensing [7], bioanalysis [8], drug delivery [9], magnetic resonance imaging (MRI) [10], and hyperthermia treatment of tumours [11].

The unique behavior and increasing applications of M(N)Ps have stimulated the advancement of new synthesis methods. The core of M(N)Ps can be made of a wide range of magnetic materials such as nickel, cobalt, iron and iron oxides. Iron oxides and their corresponding ferrites are the most commonly used due to their high magnetic moments, biological compatibility, simple synthesis and low cost of production. However, bare iron oxide nanoparticles are only stable in low ionic strength solutions at pH values above (pH 9–12) or below (pH 2–5) their point zero charge. To prevent aggregation and increase selectivity, the magnetic cores are usually coated with inorganic materials [12], polymers [13–16] and/or functionalised with organic and biological molecules [1,17]. There is a large quantity of literature exploiting the synthesis and surface engineering of M(N)Ps for many purposes. Compared to this large output, the body of reports on separation approaches used for the analysis of M(N)Ps is considerably smaller, but still very significant.

* Corresponding author. Private Bag 75, School of Natural Sciences and Australian Centre for Research on Separation Science, University of Tasmania, Hobart, 7001, Australia. Fax: +61 362262858.
E-mail address: Mirek.Macka@utas.edu.au (M. Macka).

https://doi.org/10.1016/j.trac.2019.02.026
0165-9936/

A search in Elsevier's database Scopus shows that only ca. 12% of the total publications on M(N)Ps address analytical separation techniques. Yet, the separation and analysis of M(N)Ps is critically important to obtain information on their size, shape and chemistry surface, enabling their practical use for many applications.

In 2012, Stephens et al. [18] reviewed 58 papers describing separation of M(N)Ps by means of applied magnetic fields and field gradients for improved purification and analysis [18]. The main goal of this review is to pinpoint separation techniques of M(N)Ps for the period between 2013 and June 2018, by employing three distinct types of field-flow fractionation (FFF) (magnetic FFF, asymmetrical FFF and cyclical electrical FFF), capillary electrophoresis (CE), macroscale magnetophoresis (high/low gradient magnetic separation), and microchip magnetophoresis. Analytical separation and sample preparation approaches using M(N)Ps are deemed outside the scope of our review, for which there is a large body of literature, including recent comprehensive reviews [1–3,19–23]. All the studies discussed and critically analyzed are summarized in Table 1 in terms of particle composition and size, magnetic field applied, separation principle, separation time and complexity of the infrastructures used.

2. Separations of magnetic (nano)particles

2.1. Field flow fractionation

FFF is a separation technique that uses an external field applied perpendicular to the direction of flow causing differential migration of M(N)Ps. Typically, the flow profile in a FFF channel is laminar, so particles which interact more strongly with the field are found closer to the channel walls and will move more slowly due to slower flow streams. Analytes can be separated by different mechanisms of FFF according to the type of the field applied. Typical fields include centrifugal and gravitational forces, cross flow of solvent, and thermal, electrical and magnetic gradients [24].

2.1.1. Magnetic field flow fractionation

Magnetic field flow fractionation (MFFF) has been shown to be an effective method for the separation of polydisperse suspensions of M(N)Ps when an external magnetic field is applied along a flowing channel. Rogers et al. [25] used MATLAB to simulate the separation of fluidMAG-D (starch-coated magnetite (Fe_3O_4)) M(N)Ps of sizes between 50 and 400 nm by simulating particle trajectories and magnetic forces. The results obtained from the simulation showed that M(N)Ps within the size range of interest could be separated and collected in a size dependent manner in fraction 1 (smaller sized) and fraction 2 (larger sized). To validate this model, the simulated conditions were replicated experimentally. However, the theoretical and experimental results did not agree. This inconsistency could be due to the fact that particle-particle interactions are not taken into consideration into the model. Due to the failure of the initial experiments, the same authors changed the approach to a simple magnetic coil setup composed of a tubing wrapped around a Grade N42 diametrically magnetized neodymium cylinder [25]. An inlet for both the M(N)Ps suspension and the mobile phase was inserted at the top of the magnetic coil and a single outlet at the bottom was used for the collection of magnetic particle fractions. The tubing was filled with M(N)Ps suspension. As soon as a steady state level of accumulation of M(N)Ps across the inner wall of the tubing was achieved, an initial flow rate of 0.25 mL/min was applied to wash out the M(N)Ps remaining suspended. Then, the flow rate was increased up to 50 mL/min. DLS measurements and TEM showed that the particles collected at lower flow rates were smaller than particles collected at higher flow rates. This approach was low cost and allowed the separation of polydisperse M(N)Ps by simply controlling the flow rate. However, broad size distributions were obtained. Thus, further optimisation of the system is crucial to allow for specific applications such as in biomedicine.

2.1.1.1. Magnetic quadrupole field flow fractionation. The first prototype of a magnetic quadrupole field flow fractionation (MQFFF) was developed and evaluated by Zborowski et al. [26] for continuous separation of human peripherical lymphocytes labeled with magnetic colloids. It consisted of a quadrupole electromagnet assembly of four steel pole tips with two of them opposed the magnetic north poles and the other two opposed the magnetic south poles. The electromagnet assembly was radially symmetric. The steel was magnetized by an electric current in the coils wrapped around the poles. This configuration creates a magnetic field whose magnitude increases linearly with the radial distance from the axis. This methodology is well described by Carpino et al. [27]. The results showed that the separation process was close to the predicted behavior of an ideal quadrupole magnetic field [26]. Later on, Orita et al. [28] developed a simple on-off field MQFFF to separate and quantify two distinct sub micrometer commercial M(N)Ps (90 and 200 nm) at specific magnetic field and flow conditions [28]. This on-off field MQFFF system was inspired by the system previously developed by Zborowski et al. [26]. It consisted of a separation channel volume of 0.94 mL fitted into a stainless-steel cylinder that was implemented in a flow injection setup with downstream optical detection (Fig. 1). The fractograms exhibited improved retention (98.6% vs. 53.3%) for the larger M(N)Ps (200 nm vs.90 nm) at higher flow rates (0.05 mL/min vs. 0.01 mL/min) [28]. Thus, for given field and flow conditions, the on-off field MQFFF system can be used for the quantification of retained and unretained fractions. This is useful for the separation of unwanted weakly magnetic particulate contaminants from M(N)P suspensions. Compared to the magnetic coil setup previously described, the on-off field MQFFF system requires less handling.

Moore et al. [29] used MQFFF for red blood cell (RBC, with mean diameter of 8 μm) separation as an alternative to centrifugal separation. A quadrupole field was designed having a maximum field of 1.68 T at the magnet pole tips, zero field at the aperture axis, and a nearly constant radial field gradient of 1.75 T mm^{-1} inside a cylindrical aperture. A light-scattering detector downstream of the magnet measured light attenuation caused by the cells eluting from the magnet as a function of time. The cell samples were composed of high spin RBC (obtained by chemical conversion of hemoglobin to methemoglobin - met RBC - or exposure to anoxic conditions - deoxy RBC), low spin RBC (obtained by exposure to ambient air – oxy RBC), and mixtures of deoxy RBC and white blood cells (WBC). Cell tracking velocimetry was used to measure the magnetophoretic mobility of the RBC and the results showed that the mobility depended on the presence of high-spin hemoglobin. Only high spin RBC were attracted by the magnet, while low-spin RBC demonstrated magnetic susceptibility comparable to WBC. It was also found that RBC did not elute within 15 min from the channel at flow rate $\leq$0.05 mL/min but as would be expected rapidly eluted at a higher flow rate of 2.0 mL/min. These results agreed with earlier studies on the magnetic properties of hemoglobin using other techniques [30,31]. The fractionation experiments of RBC and a RBC/WBC mixture showed that a 5×10^7/mL cell suspension pumped at 0.1 mL/min through a magnetic field of 1.5T and gradient of 1000 T m^{-1} is depleted to less than 5% of the initial RBC number concentration. The 5% residual contamination was comparable to that typically seen in WBC obtained by blood centrifugation. One advantage over blood centrifugation, is that MQFFF RBC separation can be scaled to microliter devices for RBC debulking, which can be portable and operated immediately after donation with minimal human labor.

Table 1
Particle composition and size, magnetic field applied, separation principle, separation time and complexity of the infrastructure used for M(N)Ps and magnetically susceptible RBCs between 2013 and 2018.

Particle composition	Particle size (nm)	Magnetic field applied	Separation principle	Separation time	Complexity of the infrastructure	Ref
Starch-coated magnetite (nano) particles	50–400	51 mm length Grade N42 diametrically magnetized NdFeB cylinder	MFFF	<1 h	Basic laboratory equipment	[25]
Dextran-coated magnetite nano(particles)	90 and 200	Quadrupole electromagnet	MQFFF	50 min	Stainless-steel cylinder within a quadrupole electromagnet implemented into a flow injection setup with downstream optical detection	[28]
RBCs	8000	Quadrupole magnet	MQFFF	25 min	Cylindrical flow channel centred inside of a quadrupole magnet with downstream light scattering detection	[29]
Carboxydextran-coated maghemite nanoparticles	6–60	n.a.	AF4	15 min	AF4 instrument connected to MALLS detection	[32]
Hybrid polymer magnetic micelles	54	n.a.	AF4	15 min	AF4 instrument connected to UV and MALLS detection	[33]
Lipid and polystyrene sulfonate-coated magnetite nanoparticles	50 and 100	n.a.	CyEFFF	30 min	HPLC pump connected to an EFFF channel with downstream UV detection; ac and dc voltages induced by a signal generator and a dc power supply	[34]
Polyvinylpyrrolidone (PVP)-coated magnetic particles	127	0.56 T permanent magnetic assembly consisting of two 2× 4 × 0.5 inch NdFeB blocks with a minimum gap of 5/8 inch	HGMS	1 h	HGMS instrument	[45]
Poly (diallyl dimethylammonium chloride) (PDDA) and chitosan (Chi)-coated magnetic nanoparticles	50	NdFeB permanent magnet	LGMS	6 min	Basic laboratory equipment	[46]
Poly(diallyldimethylamonium chloride) (PDDA)-coated iron oxide nanoparticles	50 nm (spherical) and 20 × 300 nm (rod-like)	Cylindrical shaped N50-graded NdBFe (1.20 T) and Alnico permanent magnet (1.45 T) with 14 mm in diameter and 15 mm in length	LGMS	6 h	Basic laboratory equipment	[48]
Bare and carboxylated iron oxide nanoparticles	7 - 13 (bare iron oxide nanoparticles) and 10 (carboxylated iron oxide nanoparticles)	n.a.	CE	12 min	CE instrument	[39]
Carboxylated iron oxide nanoparticles	75	n.a.	CE	5 min	CE instrument	[41]
Polydisperse magnetic particles	150 and 500	Permanent NbFeB magnet (6 mm length, 4 mm width, and 3 mm thickness)	Microchip magnetophoresis	15 s	Microchip fabricated in PDMS with a side permanent magnet, a Gaussmeter, and DIC detection	[49]
Iron oxide magnetic beads	5000	Soft magnetic microstructures made of a mixture of iron powder and PDMS into a prefabricated channel	Microchip magnetophoresis	<2 s	Microchip fabricated in PDMS mounted in an inverted microscope connected to a high-speed camera, placed in the center of parallel permanent magnets	[50]
Polystyrene (5000 and 11000 nm) and polyethylene (35000 nm) magnetic beads	5000, 11000, and 35000	Permanent NbFeB N42 grade cuboid magnet	Microchip magnetophoresis	15 min	Microchip fabricated in PDMS with a side permanent magnet mounted in an inverted microscope connected to a high-speed camera	[51]
Microspheres composed of styrene-maleic acid copolymer matrix encapsulating 50% by mass magnetite cores	2000, 6000 and 12000	Octupolar array of permanent magnets	Microchip magnetophoresis	10 s	Microchip fabricated in PDMS with a spiral channel centred with respect to the octupolar magnetic array	[52]
Magnetite nanoparticles	10	Permanent NbFeB magnet	Microchip magnetophoresis	>1 h	Microchip fabricated in PDMS with permanent magnet mounted in an inverted microscope connected to a high-speed camera	[53]
Magnetite-doped and uncross-linked polystyrene particles with spherical and elliptical shapes	7000	Halbach array	Microchip magnetophoresis	<2 s	Microchip fabricated in PDMS placed in the center of the Halbach array mounted in an inverted microscope connected to a high-speed camera	[54]

AF4: Asymmetrical field flow fractionation; **CE:** Capillary electrophoresis; **CyEFFF:** Cyclical electrical field flow fractionation; **HGMS:** High gradient magnetic separation; **LGMS:** Low gradient magnetic separation; **MALLS:** Multi-angle laser light scattering; **MFFF:** Magnetic field flow fractionation; **MQFFF:** Magnetic quadrupole field flow fractionation; **RBCs:** Red blood cells.

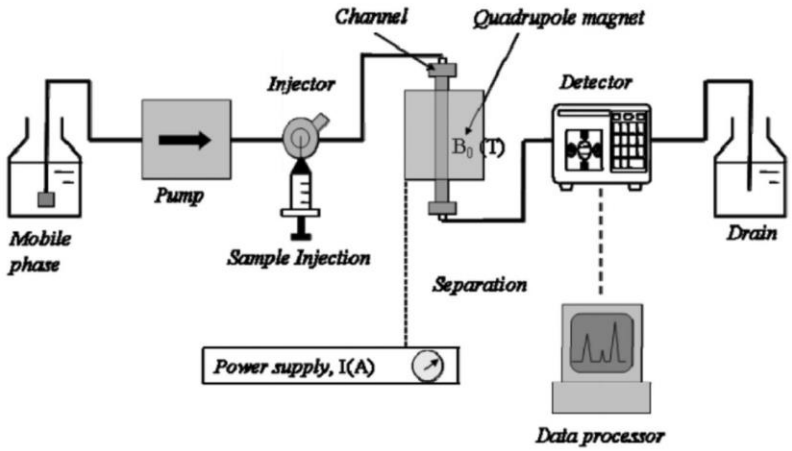

Fig. 1. Schematic of the MQFFF system. The mobile phase was driven by a pump. The sample is introduced through a separate port. The flow of the mobile phase pushes the sample from the injector into the separation channel fitted into a quadrupole electromagnet connected to a UV–visible detector. Reprinted from Ref. [28] with permission.

2.1.2. Asymmetrical flow field-flow fractionation

Asymmetrical flow field flow fractionation (AF4) is a separation technique based on the theory of FFF. The cross flow is induced by flowing liquid constantly exiting through a semi-permeable wall on the bottom of the channel. The lower size M(N)Ps, which can be fractioned, are restricted by the molecular weight cut off membrane. The suitability of AF4 has been shown for the fractionation of magneto polyplexes (with mean diameter of 54 nm) [32] and carboxydextran-coated maghemite dispersions (with diameter of 6–60 nm) [33] by connecting the AF4 instrument to UV [33] and multi-angle laser light scattering (MALLS) [32,33] detectors. AF4 can be a simple, fast and reliable tool for quality control in commercial production of M(N)Ps, while providing complementary information related to nonmagnetic sample components.

2.1.3. Cyclical electrical field flow fractionation

Cyclical electrical field flow fractionation (CyEFFF) consists of an oscillating square voltage applied between a top and bottom electrode inside the channel. As result, M(N)Ps move back and forth between the electrodes in agreement with their sizes and electrophoretic mobilities. M(N)Ps with high electrophoretic mobilities move further into the center of the channel and they spend more time at the faster fluid regions thus eluting earlier than the lower mobility M(N)Ps. One of the limitations of this technique is the band broadening of the resulting UV fractograms and low resolution. To address and solve the diffusion issue, Tasci et al. [34] reported the separation of MNPs by CyEFFF applying square wave voltages with higher duty cycles instead of DC offset voltages (Fig. 2). Thus, particle diffusion was suppressed, which allowed separations of MNPs with mean diameter of 50 and 100 nm. This study demonstrated the capability of CyEFFF for size and electrophoretic analysis of lipid and polystyrene sulfonate-coated MNPs [34].

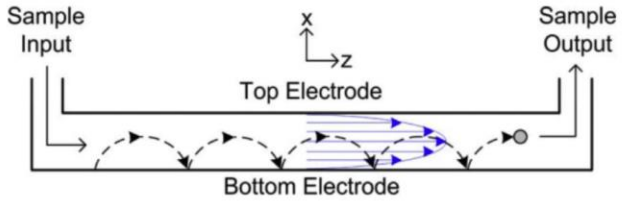

Fig. 2. Schematic of the CyEFFF system. The dashed line shows the particle trajectory that results from the cyclical electrical field. Reprinted from Ref. [34] with permission.

2.2. Capillary electrophoresis

CE is a powerful separation method which has the advantages of minimal requirement of sample and buffer volumes, and lack of generation of organic waste. Further, the use of narrow capillaries in CE with high electrical resistance, allows the application of high electrical fields with minimal heat generation. The use of high electrical fields together with the conventional plug-type flow from electrically driven systems results in short analysis times and high efficiency and resolution for almost any type of ionic analytes. Yet, a remarkable limitation of bare iron oxide M(N)P separations by CE that has been previously reported [35–38] is their high tendency to spontaneously agglomerate to minimize surface energies, which is observed in electropherograms as spurious spikes that in turn prevent the accurate determination of the electrophoretic mobilities of M(N)Ps. This limitation has been recently overcome by Alves et al. [39], who achieved symmetrical and smooth peaks of bare iron oxide nanoparticles. This was accomplished through electrostatic stabilisation using complexing electrolyte anions such as citrate and phosphate, and the additive tetramethylammonium hydroxide (TMAOH) within the background electrolyte (BGE), an ionic solution of desired concentration, co-ion and counter-ion mobilities, and usually also providing pH-buffering capacity. TMAOH is a peptizing agent (an electrolyte that converts aggregated particles into a colloidal sol) [40] used for more than two decades in the synthesis of well-dispersed iron oxide M(N)P solutions, however never utilised for effective CE separations of M(N)Ps. The same study also showed the successful separation of bare (with diameter between 7 and 13 nm) and carboxylated (10 nm) iron oxide nanoparticles in 12 min using Tris-nitrate containing 20 mM TMAOH as BGE. The electrophoretic mobilities for bare and carboxylated iron oxide nanoparticles were 3.3E-08 $m^2\ V^{-1}\ s^{-1}$ (0.9 %RSD) and 4.1E-08 $m^2\ V^{-1}\ s^{-1}$ (0.4 %RSD), respectively. These findings demonstrate that simple and rapid CE experiments are excellent tools to characterise and monitor properties and interactions of iron oxide nanoparticles with other molecules for potential surface modification purposes [39]. Baron et al. [41] studied the online stacking of carboxylated core-shell magnetite nanoparticles in CE. By monitoring the ionic strength of the BGE and the sample zone, it was observed that stacking occurred

optimally when MNPs were dispersed in 10 mM borate/NaOH (pH 9.5) and injected to the BGE composed of 100 mM borate/NaOH (pH 9.5). The decrease of the electric double layer thickness with increasing ionic strength could induce MNP aggregation and led to the restructuring of the MNPs zone due to the decrease of distance between nanoparticles [41]. The Derjaguin-Landau-Verwey-Overbeek (DLVO) theory, which describes van-der-Waals and electrostatic interactions between charged surfaces within a liquid medium [42], was suggested as a cause of peak sharpening in CE.

2.3. Macroscale magnetophoresis

Magnetophoresis refers to the motion of magnetic particles or magnetizable material through a fluid under the influence of a magnetic field [43]. For almost all the M(N)Ps applications, manipulation, recovery, and collection rates using external magnets should be done quickly. Rapid magnetophoretic separation can be attained under both high gradient (HGMS, $\nabla B^{\rightarrow} > 1000$ T m^{-1}) and low gradient magnetic separation (LGMS, $\nabla B^{\rightarrow} < 100$ T m^{-1}).

2.3.1. High gradient magnetic separation

HGMS is commonly employed in conventional industry practice to separate magnetic materials from non-magnetic aqueous solutions, such as for wastewater treatment of bacteria and solids. Typically, HGMS is used to separate microscale or bigger particles, or microscale aggregates of nanoparticles, or nanoparticles encapsulated in larger polymer beads. However, the application of HGMS to suspensions of individually dispersed M(N)Ps has been poorly explored so far. HGMS systems generally consist of a column packed with magnetically susceptible wires placed inside an electromagnet. Through application of a magnetic field across the column, the wires dehomogenise the magnetic field in the column producing high field gradients around the wires to enable the capture of M(N)Ps onto their surfaces. The attraction of M(N)Ps depends on the magnetic field gradients generated, particle size and magnetic properties [44]. A study conducted by Mirshahghassemi et al. [45] describes the application of HGMS for oil remediation using polyvinylpyrrolidone (PVP)-coated MPs (mean size diameter of 127 nm) in a continuous and large volume flow system. This technique was analyzed as a function of magnetic field strength, mixing time and stainless-steel wool content. Fluorescence and inductively coupled plasma-optical emission spectrometer (ICP-OES) data indicated that ca. 85% of oil and 95% of MNP were eliminated. The continuous use of this HGMS system over 7 h allowed the treatment of 17 L oil water mixture with no reduction of the oil and MPs removal capacity [45]. Although this study introduces a new application of HGMS for oil remediation, it has the disadvantages of being tedious and time-consuming.

2.3.2. Low gradient magnetic separation

In contrast to conventional practice where HGMS is normally employed, LGMS is still poorly explored and understood. Toh et al. [46,47] showed the reliability of LGMS for magnetophoretic separation of microalgal biomass that interacted electrostatically with cationic polymer functionalised MNPs [46,47]. Poly (diallyl dimethylammonium chloride) (PDDA) and chitosan (Chi) (with mean diameter of 50 nm) worked as binding agents to promote rapid separation of the negatively charged *Chlorella* sp. through LGMS at field gradient lower than 80 T m^{-1}. The obtained results indicated cell separation efficiency of about 98% for PDDA and 99% for Chi. Though, from a practical point of view, PDDA was preferable as polymer binder since the attachment mechanism involved was pH independent [47]. Because almost all the magnetophoretic studies have been dedicated to the behavior of spherical MNPs, and poor attention has been paid to rod-like MNPs, Lim et al. [48] compared the magnetophoretic behavior of spherical and rod-like iron oxide nanoparticles under LGMS. Both effects of particle concentration and magnetic field gradient on the separation kinetics were evaluated. It was shown that at low particle concentration, the magnetophoresis of MNPs at low magnetic gradient is significantly enhanced by particle anisotropy (non-spherical shape), with rod-like MNPs taking significantly less time than spherical MNPs to be separated [48]. New approaches for the separation of M(N)Ps according to their shape, size, and coatings, along with their unique magnetic properties will open new opportunities for M(N)Ps.

2.4. Microchip magnetophoresis

The field of microfluidics is continuously evolving as miniaturized platforms provide quick analysis with high resolution at low cost, foster portability and make use of exceptionally minute amounts of reagents. Zhang et al. [49] developed a microchip based on magnetophoresis with differential interference contrast (DIC) detection (Fig. 3A, B). The real-time moving trajectories and velocities of the MPs at different magnetic field strengths (depending on the distance to the permanent magnet) were measured based on consecutive DIC

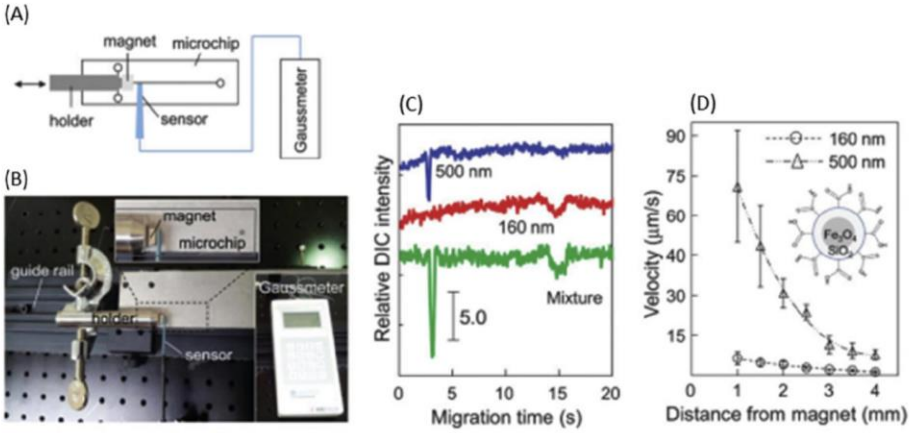

Fig. 3. Schematic diagram (A) and photography (B) of the experimental setup of the microchip magnetophoresis. (C) Representative magnetopherograms of the MPs by microchip magnetophoresis with the DIC detection system. (D) Magnetophoretic velocities of the MPs at different permanent magnet distances obtained using a DIC microscope. Reprinted from Ref. [49] with permission.

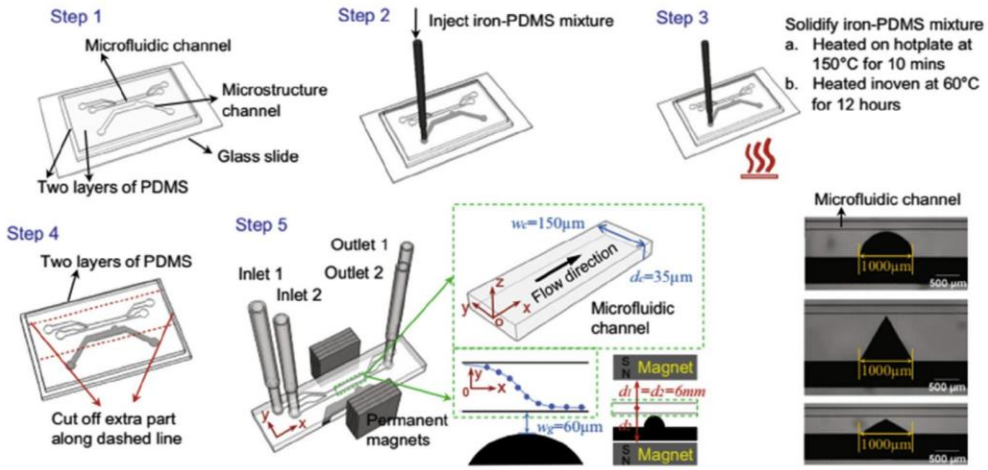

Fig. 4. Fabrication process of the microfluidic device for efficient separation of magnetic particles based on deflection in flowing streams. Reprinted from Ref. [50] with permission.

images. The results indicated that shorter distances to the magnet caused higher magnetophoretic velocities of MPs, and enhanced magnetophoretic velocity differences between dissimilar particle sizes (Fig. 3D) [49]. This study allowed the successful separation and detection of a polydisperse mixture of MPs (500 nm and 160 nm) at a single-particle level in only about 15 s (Fig. 3C).

The microfluidic separation of iron oxide beads (5 μm diameter) with soft magnetic microstructures was demonstrated by Zhou et al. [50]. The fabrication process of the microfluidic device is represented in Fig. 4. This microfluidic device consisted of two channels - fluidic and structural – made in polydimethylsiloxane (PDMS). The fluidic channel contained two inlets and two outlets. A mixture of iron powder and PDMS was injected into the structural channel located between two external permanent magnets. Three microstructure shapes were studied: (i) half circle, (ii) 60° isosceles triangle and (iii) 120° isosceles triangle. The soft magnetic microstructures provided localized and strong magnetic forces on the MPs that deflected them perpendicularly to the pressure-driven flow. Thus, the separation depended on the magnetic forces. In turn, magnetic forces are affected by the shape of the iron-PDMS microstructures and the mass ratio of the iron-PDMS composite. Also, the flow rate in the fluid channel affects the time that MPs are subjected to the magnetic field, and consequently their vertical deflection. Numerical simulations were developed to predict the particle trajectories showing good agreement with experimental data. Finally, systematic experiments and simulations were conducted to study the effect of several relevant factors on the separation of MPs: microstructure shape, mass ratio of the iron–PDMS, microfluidic channel width and average flow velocity. The results demonstrated that (i) half circular iron–PDMS microstructure caused greater deflections, (ii) larger mass ratio of the iron–PDMS composite provided higher magnetic forces, and (iii) wider channels separate MPs less efficiently than narrow microfluidic channels when operating at the same flow rate [50]. Based on the

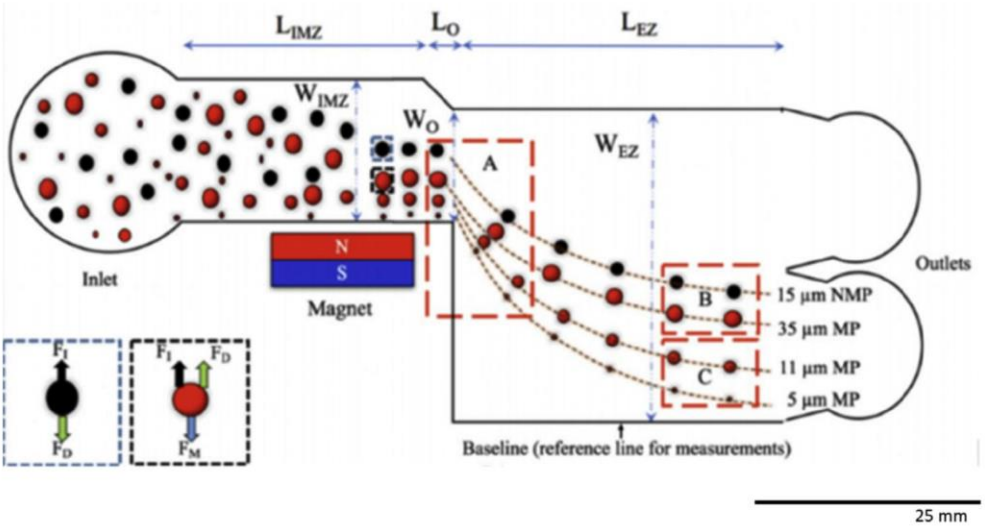

Fig. 5. MIMF scheme of the particle separation. The device (scale bar 25 mm) consisted of an inertio-magnetic zone (IMZ) with a side permanent magnet and an expansion zone (EZ). The schematic representation of MIMF device shows three red-colored magnetic particles (MP) of varied sizes and a black-colored non-magnetic particle (NMP). Reprinted from Ref. [51] with permission.

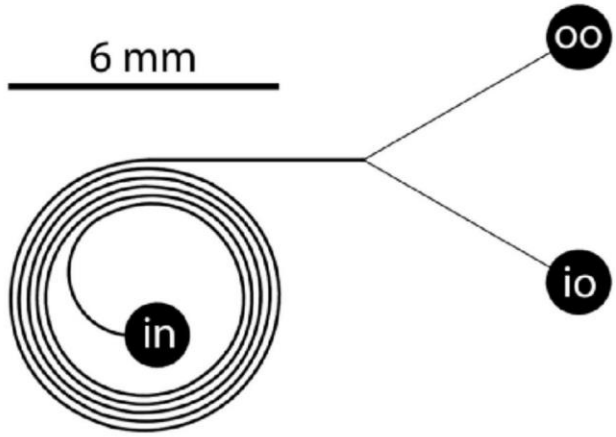

Fig. 6. Geometry of the microfluidic spiral. The fluid was injected via the input port (in) and exits through the exit ports referred as inner outlet (io) and outer outlet (oo). Reprinted from Ref. [52] with permission.

obtained results, enhanced separations of MPs can be achieved in a compact, simple and low-cost microfluidic device.

Kumar and Rezai [51] introduced a novel hybrid technique called multiplex inertio-magnetic fractionation (MIMF) to simultaneously fractionate up to four magnetic and non-magnetic particles in water at a throughput of 10^6–10^9 particles per hour. The MIMF device was based on interactions between flow-induced inertial forces and magnetic forces in an expansion microchannel containing an external permanent magnet (Fig. 5). The particle fractionation performance was first optimized in terms of flow rate and aspect ratio of the channel and particle size on duplex MIMF to understand the behavior of the particles. The obtained knowledge was then applied to demonstrate fourplex MIMF with three magnetic monodisperse particles (5, 11 and 35 μm) and nonmagnetic particles (15 μm). The non-magnetic particles inertially focus at the center of the channel, while magnetic particles get fractionated based on interaction between inertial and magnetic forces and positioned in a size related manner in the device with smaller particles located closer to the external magnet. The exit position for each particle type and size was measured with respect to the expansion region baseline since the focus of this study was only to investigate the concept of MIMF and not M(N)Ps sorting. In the future, outlets can be implemented based on the exit positions calculated. This MIMF device addresses several disadvantages of currently available magnetic fractionation devices such as low throughput, requirement of sheath flow and inability to fractionate multiple targets simultaneously [51].

Dutz et al. [52] studied the consequences of applying an external magnetic force to a suspension of MPs with diameters of 2, 6 and 12 μm circulating in a spiral microfluidic channel (Fig. 6). The fluid was injected via an input port located near the center of the spiral and exits through a symmetric flow splitter and two outlet ports. The exit ports were referred to as inner outlet and outer outlet, which collected the inner and outer halves of the fluid stream, respectively. For that purpose, an array of permanent magnets was arranged and accurately centred beneath the spiral to produce a magnetic field with octupolar symmetry. At low flow rates (5 μL/min) it was observed that 6 μm MPs clustered along a streamline near the outer wall of the spiral. At intermediate flow rates (30 μL/min), 6 μm MPs were homogeneously distributed across the width of the channel. At high flow rates (60 μL/min), 6 μm MPs were focused in clusters within the inner half of the spiral. The phenomenon observed at high flow rates was caused by hydrodynamic drag forces that induced secondary (Dean) flow in the spiral microfluidic channel. A model incorporating key forces involved in the spiral microchip was described and used to extract quantitative *in situ* information about the magnitude of local Dean drag forces from experimental data. The experimental results also showed that at low flow rates (5 μL/min) all the 12 μm MPs and one third of the 2 μm MPs were drawn toward the outer wall of the spiral and extracted from the outer outlet, whereas the remaining two thirds of the 2 μm MPs were extracted from the inner outlet. Gradually more 6 and 12 μm MPs were extracted from the inner outlet at higher flow rates. For example, all the 12 μm MPs were found to exit the inner outlet at 40 μL/min. The behavior of the smallest MPs (2 μm) was opposite of the larger particles, with less and less being extracted from the inner outlet as the flow rate increases [52].

The effective application of MNPs is highly dependent of appropriate cleaning after synthesis and/or before their use to remove solvents, excess of surfactants, byproducts and undesired impurities. Because manual cleaning is time consuming and inefficient, Cardoso et al. [53] designed, fabricated and tested a microfluidic system for the continuous cleaning and separation of MNPs (average diameter of 10 nm) synthesized by coprecipitation using NH_4OH as catalyst. First, a theoretical study was performed to optimize the geometrical configuration of the microfluidic device and the experimental conditions. The optimized microfluidic system was composed of two inlets and two outlets (Fig. 7). The cleaning solution (water, fluid A) was introduced through the inlet A and the synthesis solution with MNP (fluid B) through the inlet B. The waste fluid (fluid C) exited through the outlet C, whereas the cleaned MNPs solution (fluid D) exited though the outlet D. A permanent magnet was located near the diffusion channel to deflect the MNPs by magnetic forces from the synthesis solution to the cleaning solution (Fig. 7). Gas chromatography was performed to indirectly calculate the cleaning efficiency by measuring the decrease of the peak area of NH_4OH. The results demonstrated a cleaning efficiency of about 99.7% by controlling the fluid flows in the microfluidic system, whereas manual cleaning achieved a value of about 94.3% after cleaning six consecutive times. Both processes are time-consuming, however the

Fig. 7. Schematic of the optimized microfluidic system. Fluid A: cleaning solution; Fluid B: synthesis solution with MNPs; Fluid C: waste; Fluid D: cleaned MNPs. Channel widths (a) 600 μm; (b) 400 μm; (c) 600 μm; (d) 400 μm; diffusion channel length (e) 10 mm. Reprinted from Ref. [53] with permission.

microfluidic system offers negligible loss of MNPs and the process is performed autonomously [53].

The separation of magnetic particles with spherical (mean diameter of 7 μm) and elliptical shapes was demonstrated by Zhou et al. [54] in a simple and effective manner. The microfluidic chip consisted of two inlets and one outlet. The inlet 1 was injected with aqueous-glycerol solution that worked as buffer flow, while the inlet 2 was injected with sample particles suspended in aqueous-glycerol solution. The microfluidic device was placed in the center of a uniform magnetic field and mounted on an inverted microscope to record the trajectories of the magnetic particles. A pressure-driven flow was combined with the magnetic field applied perpendicularly to the flow direction. The results showed that the asymmetrical rotation of the ellipsoidal MPs, together with the particle-wall hydrodynamic interactions, resulted in a net lift force towards the channel center. Differently, spherical MPs remained closer to the channel wall. This uniform magnetic field technique can be applied to multiple microfluidic channels facilitating high throughput parallelization for biological and biomedical applications that require separation of shaped MPs [54].

3. Conclusion and outlook

The improvement of the existing approaches of synthetizing uniform and more monodisperse M(N)Ps has been notorious in recent years. However, even the most efficient and highly optimized protocols yield samples relatively polydisperse. This is an obstacle for some emerging applications of M(N)Ps with some specific functions, particularly in biomedical areas, as their properties are dependent. Analytical tools for M(N)Ps separation are fundamental to understand the behavior of M(N)Ps according to their size, shape and surface chemistry. This knowledge can give information on the monodispersity and purity of M(N)Ps for their ultimate practical use. Over the last 5 years, novel strategies for M(N)P separations have been reported based on FFF, macroscale magnetophoresis and CE, but the trend is toward integrating external magnetic fields onto single microfluidic structures. From about 33 journal articles that have been published in the last 5 years, 54% of them are microfluidic based. These can be easily fabricated and are inexpensive, not requiring any extra power source. Moreover, separations in microchip magnetophoresis can be easily achieved with high efficiency and throughput in the order of seconds. Real-time moving trajectories and velocities of M(N)Ps can also be monitored by means of microscope imaging that is seen as the new trend in microfluidic separation and identification of M(N)Ps.

Acknowledgements

Mirek Macka gratefully acknowledges the Australian Research Council Future Fellowship (FT120100559). Manuel Miró acknowledges financial support from the Spanish State Research Agency through project CTM2017-84763-C3-3-R (MINECO/AEI/FEDER, EU). Michael Breadmore acknowledges an Australian Research Council Future Fellowship Award (FT130100101).

References

[1] Á. Ríos, M. Zougagh, Recent advances in magnetic nanomaterials for improving analytical processes, TrAC, Trends Anal. Chem. 84 (2016) 72–83.
[2] T. Jamshaid, E.T.T. Neto, M.M. Eissa, N. Zine, M.H. Kunita, A.E. El-Salhi, A. Elaissari, Magnetic particles: from preparation to lab-on-a-chip, biosensors, microsystems and microfluidics applications, TrAC, Trends Anal. Chem. 79 (2016) 344–362.
[3] I. Vasconcelos, C. Fernandes, Magnetic solid phase extraction for determination of drugs in biological matrices, TrAC, Trends Anal. Chem. 89 (2017) 41–52.
[4] S. Miltenyi, W. Müller, W. Weichel, A. Radbruch, High gradient magnetic cell separation with MACS, Cytometry 11 (1990) 231–238.
[5] S.A. Wahajuddin, Superparamagnetic iron oxide nanoparticles: magnetic nanoplatforms as drug carriers, Int. J. Nanomed. 7 (2012) 3445.
[6] S.R. Dave, X. Gao, Monodisperse magnetic nanoparticles for biodetection, imaging, and drug delivery: a versatile and evolving technology, Wiley Interdiscip. Rev. Nanomed. Nanobiotechnol. 1 (2009) 583–609.
[7] J.M. Perez, T. O'Loughin, F.J. Simeone, R. Weissleder, L. Josephson, DNA-based magnetic nanoparticle assembly acts as a magnetic relaxation nanoswitch allowing screening of DNA-cleaving agents, J. Am. Chem. Soc. 124 (2002) 2856–2857.
[8] J.E. Smith, L. Wang, W. Tan, Bioconjugated silica-coated nanoparticles for bioseparation and bioanalysis, TrAC, Trends Anal. Chem. 25 (2006) 848–855.
[9] N. Kohler, C. Sun, J. Wang, M. Zhang, Methotrexate-modified superparamagnetic nanoparticles and their intracellular uptake into human cancer cells, Langmuir 21 (2005) 8858–8864.
[10] B. Chertok, B.A. Moffat, A.E. David, F. Yu, C. Bergemann, B.D. Ross, V.C. Yang, Iron oxide nanoparticles as a drug delivery vehicle for MRI monitored magnetic targeting of brain tumors, Biomaterials 29 (2008) 487–496.
[11] K. Maier-Hauff, F. Ulrich, D. Nestler, H. Niehoff, P. Wust, B. Thiesen, H. Orawa, V. Budach, A. Jordan, Efficacy and safety of intratumoral thermotherapy using magnetic iron-oxide nanoparticles combined with external beam radiotherapy on patients with recurrent glioblastoma multiforme, J. Neuro Oncol. 103 (2011) 317–324.
[12] V. Salgueiriño-Maceira, M.A. Correa-Duarte, M. Spasova, L.M. Liz-Marzán, M. Farle, Composite silica spheres with magnetic and luminescent functionalities, Adv. Funct. Mater. 16 (2006) 509–514.
[13] G.S. Demirer, A.C. Okur, S. Kizilel, Synthesis and design of biologically inspired biocompatible iron oxide nanoparticles for biomedical applications, J. Mater. Chem. B 3 (2015) 7831–7849.
[14] J. Chomoucka, J. Drbohlavova, D. Huska, V. Adam, R. Kizek, J. Hubalek, Magnetic nanoparticles and targeted drug delivering, Pharmacol. Res. 62 (2010) 144–149.
[15] A.K. Gupta, M. Gupta, Synthesis and surface engineering of iron oxide nanoparticles for biomedical applications, Biomaterials 26 (2005) 3995–4021.
[16] D. Singh, J.M. McMillan, X.-M. Liu, H.M. Vishwasrao, A.V. Kabanov, M. Sokolsky-Papkov, H.E. Gendelman, Formulation design facilitates magnetic nanoparticle delivery to diseased cells and tissues, Nanomedicine 9 (2014) 469–485.
[17] W. Wu, Q. He, C. Jiang, Magnetic iron oxide nanoparticles: synthesis and surface functionalization strategies, Nanoscale Res. Lett. 3 (2008) 397.
[18] J.R. Stephens, J.S. Beveridge, M.E. Williams, Analytical methods for separating and isolating magnetic nanoparticles, Phys. Chem. Chem. Phys. 14 (2012) 3280–3289.
[19] V. Tolmacheva, V. Apyari, E. Kochuk, S. Dmitrienko, Magnetic adsorbents based on iron oxide nanoparticles for the extraction and preconcentration of organic compounds, J. Anal. Chem. 71 (2016) 321–338.
[20] Y. Wang, Q. Chen, C. Gan, B. Yan, Y. Han, J. Lin, A review on magnetophoretic immunoseparation, J. Nanosci. Nanotechnol. 16 (2016) 2152–2163.
[21] A.A. Hernandez-Hernandez, G.A. Alvarez-Romero, E. Contreras-Lopez, K. Aguilar-Arteaga, A. Castaneda-Ovando, Food analysis by microextraction methods based on the use of magnetic nanoparticles as supports: recent advances, Food Anal. Methods 10 (2017) 2974–2993.
[22] S. Piovesana, A.L. Capriotti, Magnetic materials for the selective analysis of peptide and protein biomarkers, Curr. Med. Chem. 24 (2017) 438–453.
[23] T. Tangchaikeeree, D. Polpanich, A. Elaissari, K. Jangpatarapongsa, Magnetic particles for *in vitro* molecular diagnosis: from sample preparation to integration into microsystems, Colloids Surf., B 158 (2017) 1–8.
[24] J.C. Giddings, F. Yang, M.N. Myers, Flow-field-flow fractionation: a versatile new separation method, Science 193 (1976) 1244–1245.
[25] H.B. Rogers, T. Anani, Y.S. Choi, R.J. Beyers, A.E. David, Exploiting size-dependent drag and magnetic forces for size-specific separation of magnetic nanoparticles, Int. J. Mol. Sci. 16 (2015) 20001–20019.
[26] M. Zborowski, L. Sun, L.R. Moore, P.S. Williams, J.J. Chalmers, Continuous cell separation using novel magnetic quadrupole flow sorter, J. Magn. Magn. Mater. 194 (1999) 224–230.
[27] F. Carpino, L.R. Moore, J.J. Chalmers, M. Zborowski, P.S. Williams, Quadrupole Magnetic Field-Flow Fractionation for the Analysis of Magnetic Nanoparticles, IOP Publishing., 2005, p. 174.
[28] T. Orita, L.R. Moore, P. Joshi, M. Tomita, T. Horiuchi, M. Zborowski, A quantitative determination of magnetic nanoparticle separation using on-off field operation of quadrupole magnetic field-flow fractionation (QMgFFF), Anal. Sci. 29 (2013) 761–764.
[29] L.R. Moore, P.S. Williams, F. Nehl, K. Abe, J.J. Chalmers, M. Zborowski, Feasibility study of red blood cell debulking by magnetic field-flow fractionation with step-programmed flow, Anal. Bioanal. Chem. 406 (2014) 1661–1670.
[30] L. Pauling, C.D. Coryell, The magnetic properties and structure of hemoglobin, oxyhemoglobin and carbonmonoxyhemoglobin, Proc. Natl. Acad. Sci. U.S.A. 22 (1936) 210–216.
[31] C.D. Coryell, F. Stitt, L. Pauling, The magnetic properties and structure of ferrihemoglobin (methemoglobin) and some of its compounds, J. Am. Chem. Soc. 59 (1937) 633–642.
[32] E. Wetterskog, A. Castro, L. Zeng, S. Petronis, D. Heinke, E. Olsson, L. Nilsson, N. Gehrke, P. Svedlindh, Size and property bimodality in magnetic nanoparticle dispersions: single domain particles vs. strongly coupled nanoclusters, Nanoscale 9 (2017) 4227–4235.

[33] E. Haladjova, S. Rangelov, M. Geisler, S. Boye, A. Lederer, G. Mountrichas, S. Pispas, Asymmetric flow field-flow fractionation investigation of magnetopolyplexes, Macromol. Chem. Phys. 216 (2015) 1862–1867.
[34] T. Tasci, E. Manangon, D. Fernandez, W. Johnson, B. Gale, Separation of magnetic nanoparticles by cyclical electrical field flow fractionation, IEEE Trans. Magn. 49 (2013) 331–335.
[35] G.R. Ducatte, N.E. Ballou, C. Quang, S.L. Petersen, Separation and characterization of oxide particles by capillary electrophoresis, J. Microcolumn Sep. 8 (1996) 403–412.
[36] C. Quang, S. Petersen, G. Ducatte, N. Ballou, Characterization and separation of inorganic fine particles by capillary electrophoresis with an indifferent electrolyte system, J. Chromatogr. A 732 (1996) 377–384.
[37] S.L. Petersen, N.E. Ballou, Separation of micrometer-size oxide particles by capillary zone electrophoresis, J. Chromatogr. A 834 (1999) 445–452.
[38] N.G. Vanifatova, B.Y. Spivakov, J. Mattusch, U. Franck, R. Wennrich, Investigation of iron oxide nanoparticles by capillary zone electrophoresis, Talanta 66 (2005) 605–610.
[39] M.N. Alves, P.N. Nesterenko, B. Paull, P.R. Haddad, M. Macka, Separation of superparamagnetic magnetite nanoparticles by capillary zone electrophoresis using non-complexing and complexing electrolyte anions and tetramethylammonium as dispersing additive, Electrophoresis 39 (2018) 1429–1436.
[40] F. Mérida, A. Chiu-Lam, A.C. Bohórquez, L. Maldonado-Camargo, M.-E. Pérez, L. Pericchi, M. Torres-Lugo, C. Rinaldi, Optimization of synthesis and peptization steps to obtain iron oxide nanoparticles with high energy dissipation rates, J. Magn. Magn. Mater. 394 (2015) 361–371.
[41] D. Baron, P. Dolanská, Z. Medříková, R. Zbořil, J. Petr, On-line stacking of carboxylated magnetite core–shell nanoparticles in capillary electrophoresis, J. Sep. Sci. 40 (2017) 2482–2487.
[42] M. Boström, V. Deniz, G. Franks, B. Ninham, Extended DLVO theory: electrostatic and non-electrostatic forces in oxide suspensions, Adv. Colloid Interface Sci. 123 (2006) 5–15.
[43] M. Zborowski, J.J. Chalmers, Magnetophoresis: Fundamentals and Applications, Wiley Encyclopedia of Electrical and Electronics Engineering, 1999, pp. 1–23.
[44] G.D. Moeser, K.A. Roach, W.H. Green, T. Alan Hatton, P.E. Laibinis, High-gradient magnetic separation of coated magnetic nanoparticles, AlChE J. 50 (2004) 2835–2848.
[45] S. Mirshahghassemi, A.D. Ebner, B. Cai, J.R. Lead, Application of high gradient magnetic separation for oil remediation using polymer-coated magnetic nanoparticles, Separ. Purif. Technol. 179 (2017) 328–334.
[46] P.Y. Toh, B.W. Ng, C.H. Chong, A.L. Ahmad, J.-W. Yang, C.J.C. Derek, J. Lim, Magnetophoretic separation of microalgae: the role of nanoparticles and polymer binder in harvesting biofuel, RSC Adv. 4 (2014) 4114–4121.
[47] P.Y. Toh, B.W. Ng, A.L. Ahmad, D.C.J. Chieh, J. Lim, Magnetophoretic separation of Chlorella sp.: role of cationic polymer binder, Process Saf. Environ. Protect. 92 (2014) 515–521.
[48] J. Lim, S.P. Yeap, C.H. Leow, P.Y. Toh, S.C. Low, Magnetophoresis of iron oxide nanoparticles at low field gradient: the role of shape anisotropy, J. Colloid Interface Sci. 421 (2014) 170–177.
[49] P. Zhang, S. Park, S.H. Kang, Size-dependent magnetophoresis of native single super-paramagnetic nanoparticles in a microchip, Chem. Commun. 49 (2013) 7298–7300.
[50] R. Zhou, C. Wang, Microfluidic separation of magnetic particles with soft magnetic microstructures, Microfluid. Nanofluidics 20 (2016) 48.
[51] V. Kumar, P. Rezai, Multiplex Inertio-Magnetic Fractionation (MIMF) of magnetic and non-magnetic microparticles in a microfluidic device, Microfluid. Nanofluidics 21 (2017) 83.
[52] S. Dutz, M. Hayden, U. Häfeli, Fractionation of magnetic microspheres in a microfluidic spiral: interplay between magnetic and hydrodynamic forces, PLoS One 12 (2017), e0169919.
[53] V. Cardoso, D. Miranda, G. Botelho, G. Minas, S. Lanceros-Méndez, Highly effective clean-up of magnetic nanoparticles using microfluidic technology, Sensor. Actuator. B Chem. 255 (2018) 2384–2391.
[54] R. Zhou, F. Bai, C. Wang, Magnetic separation of microparticles by shape, Lab Chip 17 (2017) 401–406.

Chapter 2. Separation of Superparamagnetic Magnetite Nanoparticles by Capillary Zone Electrophoresis using Non-complexing and Complexing Electrolyte Anions and Tetramethylammonium as Dispersing Additive

*The research contained in this chapter has been published as Alves, M. N., Nesterenko, P. N., Paull, B., Haddad, P. R., Macka, M. Separation of superparamagnetic magnetite nanoparticles by capillary zone electrophoresis using non-complexing and complexing electrolyte anions and tetramethylammonium as dispersing additive. *Electrophoresis* **2018**, 39, 1429-1436.

Chapter 2 has been removed for copyright or proprietary reasons.

It is the following published article: Alves, M. N., Nesterenko, P. N., Paull, B., Haddad, P. R., Macka, M. 218. Separation of superparamagnetic magnetite nanoparticles by capillary zone electrophoresis using non-complexing and complexing electrolyte anions and tetramethylammonium as dispersing additive, Electrophoresis, 39(12), 1429-1436

Supplementary Information

Separation of superparamagnetic magnetite nanoparticles by capillary zone electrophoresis using non-complexing and complexing electrolyte anions and tetramethylammonium as dispersing additive

Monica N. Alves[1], Pavel N. Nesterenko[1], Brett Paull[1], Paul R. Haddad[1], Mirek Macka[1]*

[1] School of Natural Sciences and Australian Centre for Research on Separation Science (ACROSS), University of Tasmania, Hobart 7001, Australia

*Corresponding author

Professor Mirek Macka, Private Bag 75, School of Physical Sciences and Australian Centre for Research on Separation Science, University of Tasmania, Hobart 7001, Australia

E-mail: Mirek.Macka@utas.edu.au

Phone: +61 362266670; Fax: +61 362262858

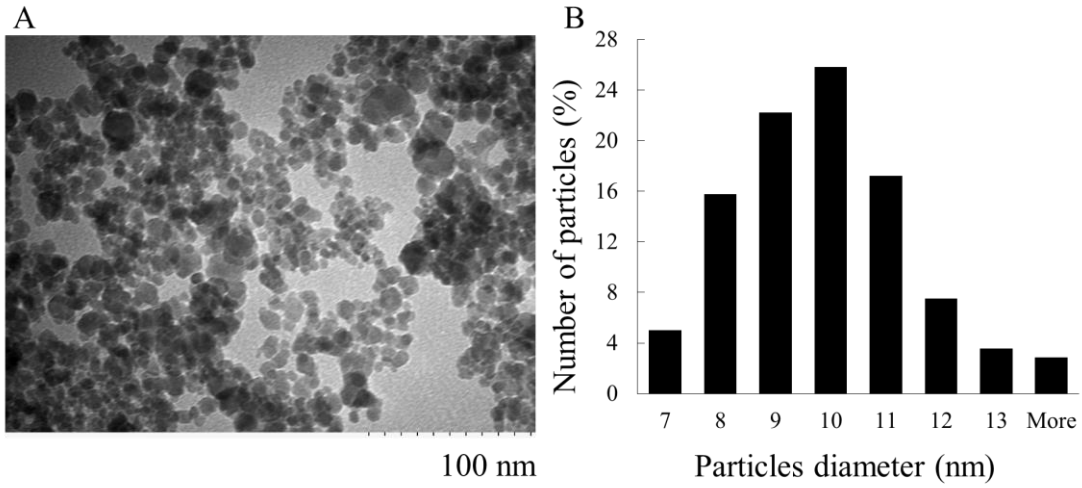

Figure S1 – Suspensions of 0.01% (w/v) BSPMNPs in water. (A) TEM image. (B) Size distribution.

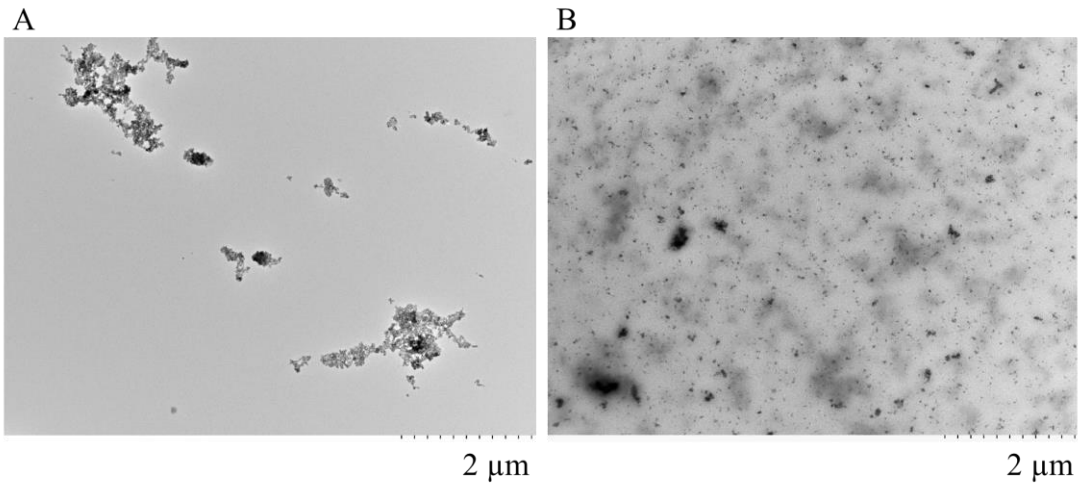

Figure S2 –TEM images of suspensions of 0.01% (w/v) BSPMNPs in different BGEs. (A) 10 mM Tris-nitrate (pH 9.00). (B) 10 mM Tris-nitrate containing 20 mM of TMAOH (pH 12.70).

Table S1 – Physicochemical properties of the nanoparticles in study including the average radius, volume, surface area and mass of a single BSPMNP, average true density and number of injected BSPMNPs.

BSPMNP radius (nm)	Volume of a BSPMNP (nm^3)	Surface area of a BSPMNP (nm^2)	BSPMNPs density (g/cm^3)*	Mass of a BSPMNP (ng)	Mass of BSPMNPs injected (ng)	Number of BSPMNPs injected
5.50E+00	6.97E+02	3.80E+02	4.95E+00	3.45E-09	3.30E+01	9.57E+09

*According to the product datasheet for nanoparticles (Fe_3O_4, high purity, 99.5+%), US Research Nanomaterials, Inc. (Houston, USA).

Chapter 3. Online Magnetic Capture of Bare Superparamagnetic Magnetite Nanoparticles in a Capillary Electrophoresis System

Abstract

The magnetic capture of bare superparamagnetic magnetite nanoparticles (BSPMNPs) electrically driven at constant voltage of 15 kV and pressure driven at 40 mbar in a fused silica capillary of 60 cm total length and 75 μm id was investigated. It was found that when 4 square NdFeB magnets are sequentially positioned within a capillary zone, and BSPMNPs flow by pressure, ca 68% of them are captured, corresponding to 20% higher capture than electrically driven BSPMNPs. In addition, it has been demonstrated that a single layer magnetic coil (4 to 43 cm) of copper wire is ineffective for BSPMNPs capture. The findings of this study can be used in the future to design magnetic fields (permanent magnets or electromagnets) for more effective nanoparticle's capture.

3.1 Introduction

Magnetophoresis is a well-known technique in biotechnology since it provides a rapid and convenient method to enrich cells of interest from a heterogeneous cell population, and to separate and purify bio-analytes grafted on magnetic carriers [1-3]. Another recent application of magnetophoresis is therapeutic delivery through blood flow. Seeking for a better understanding of the dynamics of magnetic nano-/microparticles capture in a flow, diverse authors suggest optimal orientation of permanent magnets near a

capillary [4] as well as ideal flow rates [5-6]. Kikura *et al*. also monitored capillary blocking caused by clusters of ferromagnetic nanoparticles to understand possible variants that lead to embolism [7].

Capillary electrophoresis (CE) has been used as a powerful separation method in a wide range of applications from biological macromolecules to small-molecule pharmaceuticals. Yet, one major drawback of CE is its low sensitivity. Therefore, efficient online or offline sample preconcentration is usually required [8]. Various preconcentration strategies based on electrokinetic stacking or focalization, or via liquid-liquid systems and solid phase extraction can be found in recent reviews [9-10]. Magnetic solid phase extraction prior CE analysis using functionalised magnetic nanoparticles is gaining popularity due to its high extraction efficiency and convenience of operation [11-13]. However, its implementation for online preconcentration in CE is limited. To develop insights on this topic, here, a method has been shown to capture BSPMNPs (average 11 nm) in a CE using external magnets and a magnetic coil. This Chapter also compares, for the first time in a CE instrument, the efficiency in capturing magnetic nanoparticles under pressure and electrically driven flow profiles.

3.2 Experimental

3.2.1 Reagents

Commercial iron oxide nanoparticles Fe_3O_4, high purity, 99.5+% were purchased from US Research Nanomaterials, Inc and sodium phosphate monobasic ≥99.0% and sodium phosphate dibasic ≥99.5% were purchased from Sigma-Aldrich. Milli-Q Millipore Gradient System (Millipore SAS) was used for all solutions preparation.

3.2.2 Instrumentation

Experiments were performed using an Agilent 7100 CE system with a diode array detector (Agilent Technologies). Absorbance was monitored at 254 nm at a data acquisition rate of 40 Hz. Data acquisition was performed using OpenLAB CDS ChemStation software. All reported results were obtained from at least 3 repetitions. Fused-silica capillaries (Polymicro Technologies, Phoenix, AZ, USA) of 75 µm ID and 365 µm OD with a total length of 65 cm were used in this study. Detection windows were burned with a butane torch at 8.5 cm from the capillary end.

3.2.3 Capillary electrophoresis conditions

New capillaries were pre-treated with 0.5 M NaOH for 10 min, followed by water for 10 min, and finally the electrolyte for 10 min. The temperature was kept at 25°C in all experiments. All samples contained 0.1% (w/v) of BSPMNPs dispersed in the electrolyte. Prior to each run the particle suspensions were ultrasonicated for 7 min. Hydrodynamic injections were performed at 5 kPa for 5 seconds. In order to wash the trapped BSPMNPs, prior to each run, the external magnets were removed from the experimental set up and the capillary was conditioned by flushing water for 3 min, 0.5 M NaOH for 2 min, water for 2 min, and the BGE for 2 min.

3.2.4 External permanent magnets and magnetic coil setup

Square NdFeB magnets (5 x 5 x 5 mm) were placed in contact with a capillary at approximately 18 cm from the injection end of the capillary. A 0.22 mm diameter polyurethane enamelled copper wire winding around a fused silica capillary in single layer and 4 cm length was connected to a Dick Smith Electronics 0-30V 2.5 DC Power

Supply, Model Q1770. The voltage produced at a specific current was measured using a Tenma – 72-7925 – Multimeter.

3.3 Results and discussion

CE separations of BSPMNPs were previously shown in Chapter 2 using phosphate as complexing electrolyte anion. To carry out CE under a magnetic field and analyse the capture of BSPMNPs, a length of capillary was placed in contact with the top edge of square NdFeB magnets (**Fig. 3.1**) placed at approximately 18 cm from the injection end of the capillary. This configuration caused magnetic forces proportional to the gradient in magnetic field.

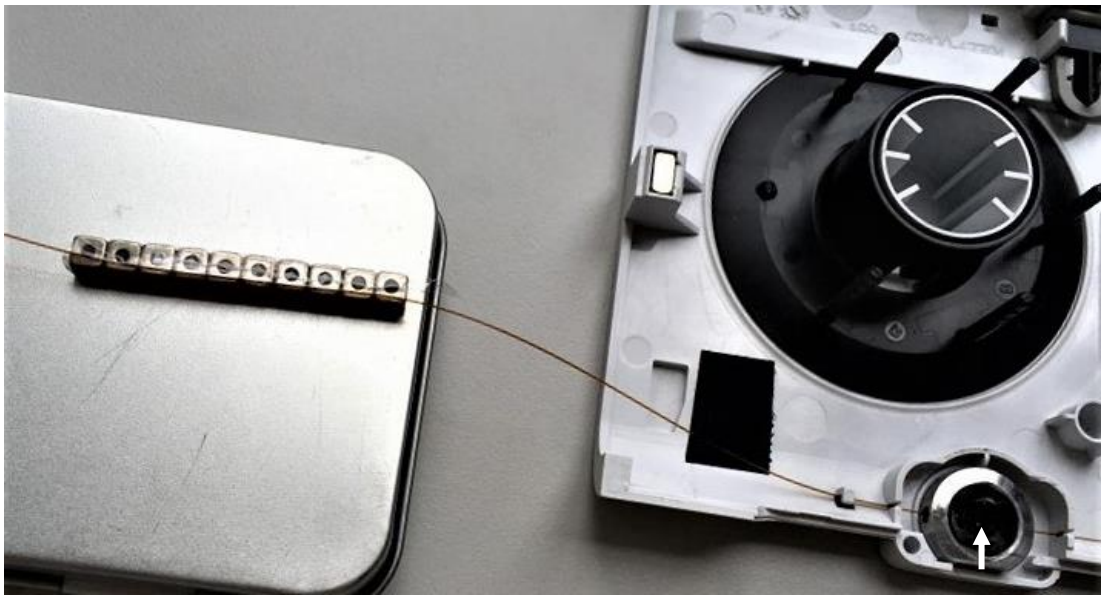

Fig. 3.1 Cassette for the Agilent 7100 CE system with square NdFeB magnets attached to a fused silica capillary. The white arrow indicates the location of the detection window.

When an external magnetic field is applied by adding 0 to 4 square NdFeB magnets (5 x 5 x 5 mm), the BSPMNPs signal declines with the number of NdFeB magnets

adjacent to the fused silica capillary with maximum depletion of BSPMNPs at 10 square NdFeB magnets (**Fig. 3.2**).

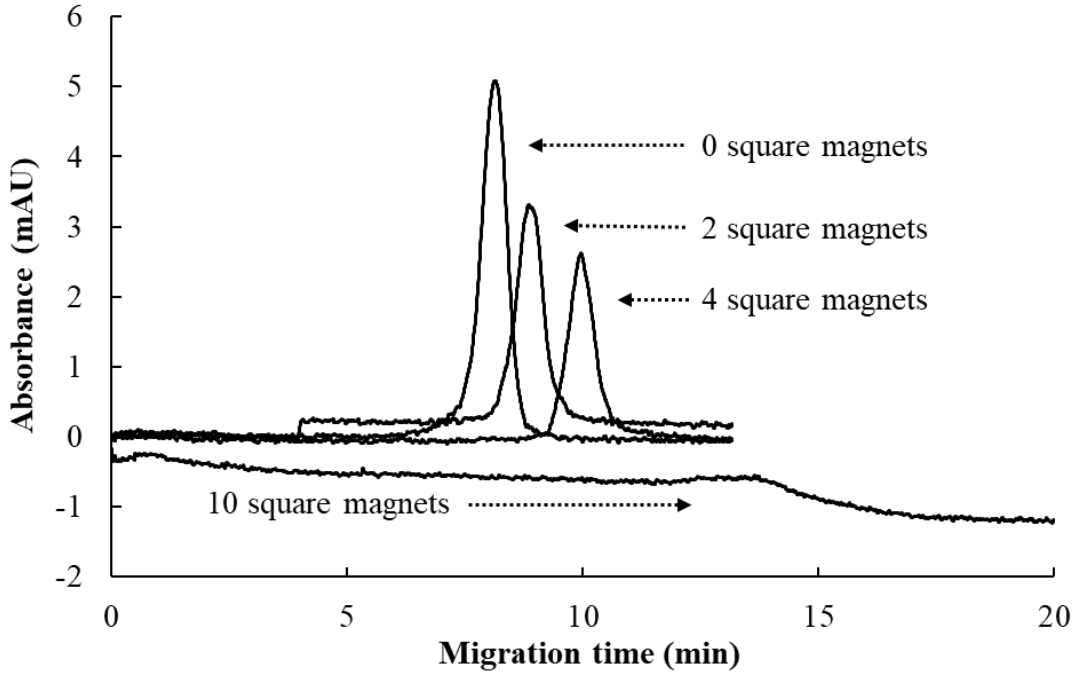

Fig. 3.2 Effect of an external magnet field consisting of 0 to 4 square NdFeB magnets on the peak area of BSPMNPs electrically driven at 15 kV. Conditions: 60 cm x 75 µm i.d. fused silica capillary (51.5 cm to the detector), 10 mM sodium phosphate, pH 7.8.

To compare the susceptibility of BSPMNPs to an external magnetic field under a parabolic profile (typical from pressure driven separations) and a plug-like profile (typical from electric driven separations), 40 mbar (pressure required to obtain the same migration time of BSPMNPs separated by CE at 15 kV, i.e. 8.1 min) was applied from the inlet extremity of the capillary to the outlet in the presence of 0 to 4 square NdFeB magnets (**Fig. 3.3**). In a hydrodynamic flow profile, the linear velocity near the capillary walls is lower than the centre of the capillary caused by friction from the walls, whereas an electroosmotic flow has a flat front since water molecules move evenly toward the cathode.

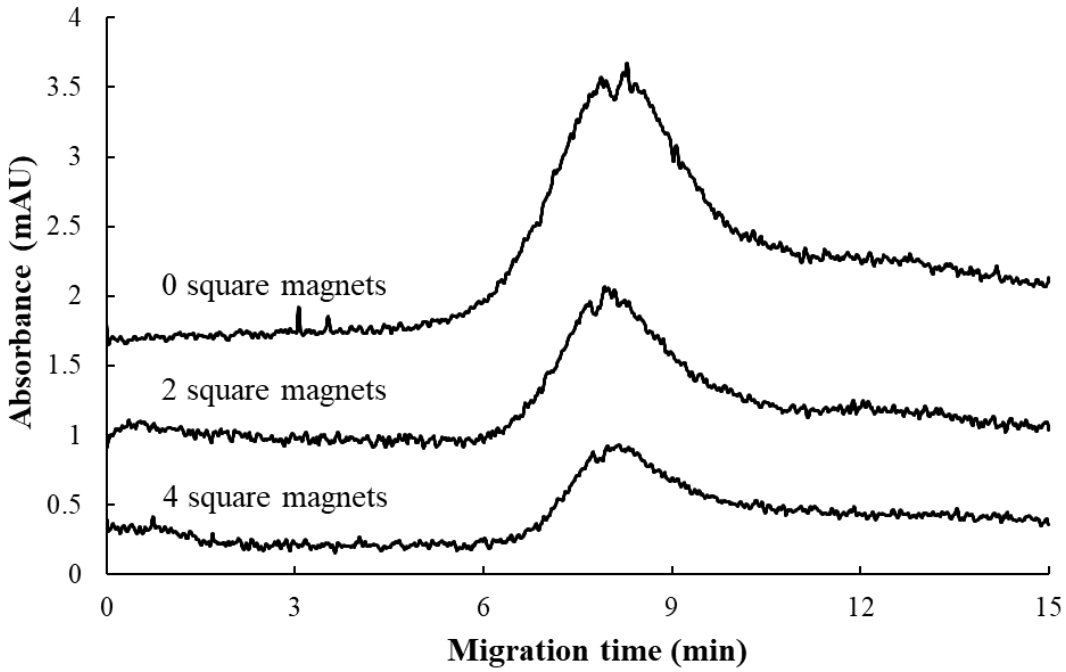

Fig. 3.3 Effect of an external magnet field consisting of 0 to 4 square NdFeB magnets on the peak area of BSPMNPs pressure driven at 40 mbar. Conditions: 60 cm x 75 µm i.d. fused silica capillary (51.5 cm to the detector), 10 mM sodium phosphate, pH 7.8.

The results have shown that when 4 square NdFeB magnets are applied, there is depletion of BSPMNPs to 53% (i.e. 47% of captured BSPMNPs) and 32% (i.e. 68% of captured BSPMNPs) for electrically driven (n=3) and pressure driven (n=3) BSPMNPs, respectively, indicating that BSPMNPs are more effectively trapped under a hydrodynamic flow profile. The lower velocity of BSPMNPs at the capillary wall, and therefore longer contact time between the BSPMNPs and the magnetic capillary zone, allows the magnetic moment of nanoparticles align with the applied magnetic field causing more effective capture.

The BSPMNPs capture under an external permanent magnetic field was successful, yet the setup was tedious and time-consuming as NdFeB magnets were attached and detached from the capillary to wash the trapped BSPMNPs every run. To automate

this process more, a magnetic coil was made using copper wire as a conductor and winding it around a fused silica capillary in single layer. The magnetic coil was 4 cm long and connected to a power supply (**Fig. 3.4A**). However, the developed magnetic coil could only generate a weak magnetic field preventing its use for CE trapping of BSPMNPs. Therefore, a longer magnetic coil covering about 43 cm of the fused silica capillary from the window to the outlet extremity was used (**Fig. 3.4B**). However, the increase in magnetic coil length was ineffective for BSPMNPs capture. The setting of the magnetic coil to the CE system is demonstrated in **Fig. 3.4C**.

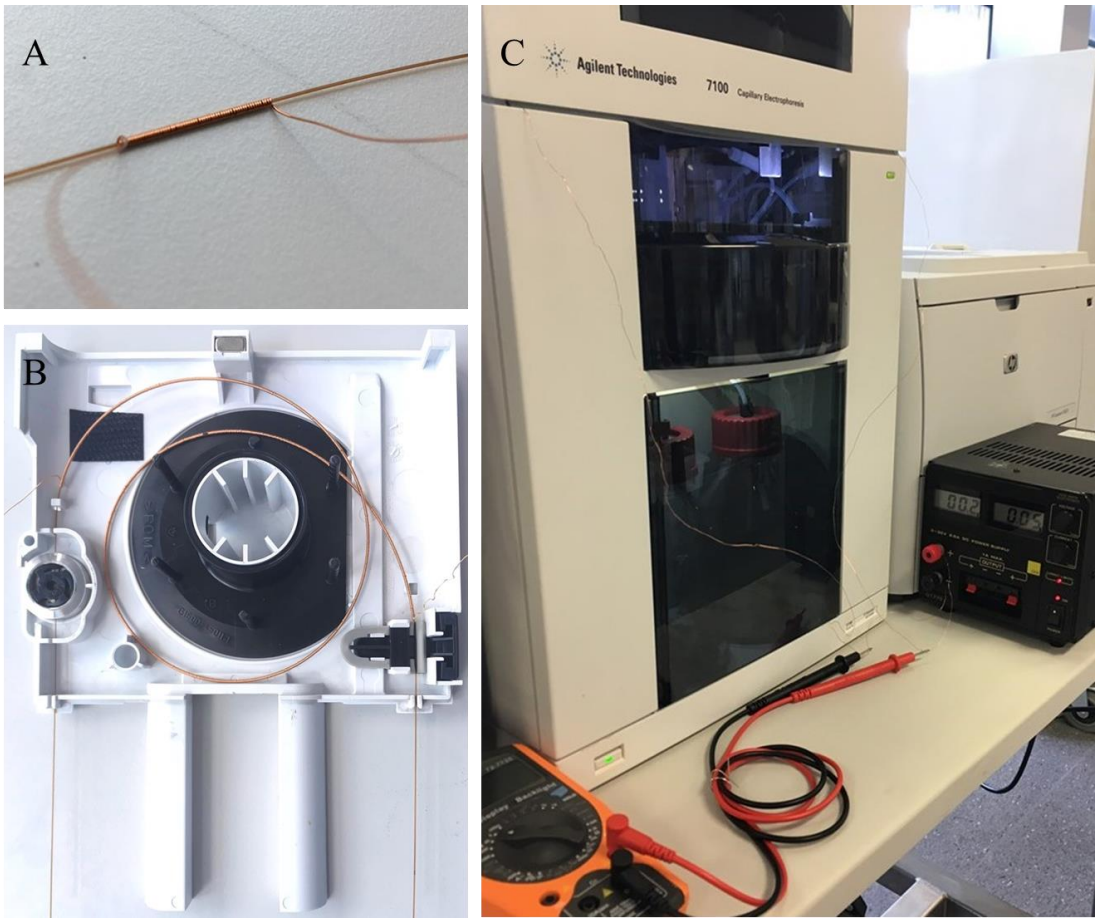

Fig 3.4 Copper wire coiled winding a fused silica capillary at different lengths (A and B) and experimental setup of the CE system coupled with a magnetic coil (C).

3.4 Conclusion

A magneto-CE system with magnetic forces proportional to the gradient in magnetic field was developed and successfully demonstrated for magnetic trapping of BSPMNP. Yet, there are magnetic configurations that would yield much higher forces than a raw of co-oriented magnets with all the poles pointing up. One example is the Halbach array. The Halbach array is a special arrangement of permanent magnets that boosts the magnetic field in one side of the array (working face), becoming up to twice as strong, while cancelling the field to near zero on the other side (non-working face). Essentially, the magnetic field that would normally be present on the non-working face is routed to the working face. This is achieved by having a spatially rotating pattern of magnetisation. In further experiments, it is aimed to test the effectivity of a Halbach array on magnetic trapping of BSPMNP.

The developed magnetic coil was ineffective for BSPMNPs capture. In the future, it is expected to build a magnetic coil with several loops of copper wire around a fused silica capillary and a core made of iron to concentrate and amplify the magnetic field. If BSPMNPs are perfectly captured using the two above mentioned approaches, the next steps are (1) magnetic trapping of functionalised particles for preconcentration purposes and (2) potential separation of metalloproteins and other magnetic susceptible compounds, which was the initial plan of the current chapter.

3.5 References

1. Hütten, A.; Sudfeld, D.; Ennen, I.; Reiss, G.; Hachmann, W.; Heinzmann, U.; Wojczykowski, K.; Jutzi, P.; Saikaly, W.; Thomas, G., New magnetic nanoparticles for biotechnology. *J. Biotechnol.* **2004,** *112* (1-2), 47.

2. McCloskey, K. E.; Moore, L. R.; Hoyos, M.; Rodriguez, A.; Chalmers, J. J.; Zborowski, M., Magnetophoretic cell sorting is a function of antibody binding capacity. *Biotechnol. Progr.* **2003,** *19* (3), 899.

3. McCloskey, K. E.; Chalmers, J. J.; Zborowski, M., Magnetic cell separation: characterization of magnetophoretic mobility. *Anal. Chem.* **2003,** *75* (24), 6868.

4. Watarai, H.; Namba, M., Capillary magnetophoresis of human blood cells and their magnetophoretic trapping in a flow system. *J. Chromatogr. A* **2002,** *961* (1), 3.

5. Hallmark, B.; Darton, N.; Han, X.; Palit, S.; Mackley, M.; Slater, N., Observation and modelling of capillary flow occlusion resulting from the capture of superparamagnetic nanoparticles in a magnetic field. *Chem. Eng. Sci.* **2008,** *63* (15), 3960.

6. Darton, N. J.; Hallmark, B.; Han, X.; Palit, S.; Slater, N. K.; Mackley, M. R., The in-flow capture of superparamagnetic nanoparticles for targeting therapeutics. *Nanomedicine: Nanotechnology, Biology and Medicine* **2008,** *4* (1), 19.

7. Kikura, H.; Matsushita, J.; Kakuta, N.; Aritomi, M.; Kobayashi, Y., Cluster formation of ferromagnetic nano-particles in micro-capillary flow. *J. Mater. Process. Technol.* **2007,** *181* (1), 93.

8. Harstad, R. K.; Johnson, A. C.; Weisenberger, M. M.; Bowser, M. T., Capillary electrophoresis. *Anal. Chem.* **2015,** *88* (1), 299.

9. Ramautar, R.; Somsen, G. W.; de Jong, G. J., Developments in coupled solid‐phase extraction–capillary electrophoresis 2013–2015. *Electrophoresis* **2016,** *37* (1), 35.

10. Breadmore, M. C.; Grochocki, W.; Kalsoom, U.; Alves, M. N.; Phung, S. C.; Rokh, M. T.; Cabot, J. M.; Ghiasvand, A.; Li, F.; Shallan, A. I., Recent advances in

enhancing the sensitivity of electrophoresis and electrochromatography in capillaries and microchips (2016–2018). *Electrophoresis* **2019,** *40* (1), 17.

11. Wierucka, M.; Biziuk, M., Application of magnetic nanoparticles for magnetic solid-phase extraction in preparing biological, environmental and food samples. *TrAC, Trends Anal. Chem.* **2014,** *59*, 50.

12. Ríos, Á.; Zougagh, M., Recent advances in magnetic nanomaterials for improving analytical processes. *TrAC, Trends Anal. Chem.* **2016,** *84*, 72.

13. Vasconcelos, I.; Fernandes, C., Magnetic solid phase extraction for determination of drugs in biological matrices. *TrAC, Trends Anal. Chem.* **2017,** *89*, 41.

Chapter 4. Recent Developments in Capillary Electrophoresis of Prokaryotes and Eukaryotes

Abstract

In aqueous buffer solutions, cells exhibit an electric surface charge due to exposed charged or chargeable functional groups. Therefore, cells can migrate in solution under the influence of an electric field. The present chapter discusses advances in CE of prokaryotic and eukaryotic cells over the past 8 years.

4.1 Introduction

All bacteria and mammalian cells have a cell membrane, which consists of lipids and proteins. The fundamental structure of the membrane is the phospholipid bilayer, which separates the cell from the surrounding environment. Proteins embedded within the phospholipid bilayer carry out specific functions, including selective transport of molecules and cell-cell recognition. Just outside of the cell membrane, most of prokaryotes, algae, fungi and some eukaryotes, including plants but not animals, present a cell wall that typically provides the cell with both structural integrity and protection [1]. Usually, the cell surface of bacteria and mammalian cells are charged. Their charge can be conferred by protonation and deprotonation of surface molecules, or adsorption of ions from the surrounding solution. Thus, prokaryotic and eukaryotic cells can migrate under the influence of an electric field [2-6]. Sophisticated instrumental techniques based on capillary electrophoresis (CE) seem to be promising for rapid and high efficiency separations of cells with minimum sample preparation and consumption. Several CE modes will be mentioned in this chapter such as capillary

zone electrophoresis (CZE) [7], micellar electrokinetic chromatography (MEKC) [8], capillary isoelectric focusing (CIEF) [9], and capillary isotachophoresis (CITP) [10-11], for a spectrum of novel applications [12-13].

Among all CE modes, CZE is the most commonly used. It separates analytes based on differences in electrophoretic mobility, which is directly proportional to the charge of the molecule, and inversely proportional to the viscosity of the solvent and radius of the molecule/particle [7]. The basic set-up for MEKC is the same as that used in CZE. The difference is that a surfactant is added to the electrolyte, above the critical micelle concentration (CMC), to form micelles. The charged surfactant micelles are attracted to an electrode at a different speed to the electroosmotic flow. The analytes are separated by differential partitioning between surfactant micelles and the surrounding electrolyte according to their hydrophobicity or hydrophilicity [8]. CIEF is a technique used to separate zwitterionic molecules i.e. molecules containing both positive and negative charges (e.g. peptides and proteins). The charge of these molecules depends on the functional groups attached to the main chain and the surrounding pH. The molecule has no net charge when the surrounding pH equals to the molecules' pI, and it is positively/negatively charged at pH lower/higher than the molecules' pI. Thus, a pH gradient is used to separate molecules in a mixture in CIEF. When voltage is applied, ions migrate according to their pI allowing for their distinct detection [9]. ITP separates charged components based on the ionic mobility in a discontinuous electrolyte system. The sample is introduced between the leading electrolyte (LE) and the terminating electrolyte (TE). If sample anions are being determined, the LE must contain an anion of higher mobility than the sample anions of interest, whereas the TE must contain an anion of lower mobility than the sample anions of interest. When an

electric field is applied, the negatively charged anions arrange themselves in order of mobility (higher to lower), between the TE and the LE, and each individual anionic sample component moves separately as a pure band [10-11].

This chapter follow the reviews of Subirats *et al*. [5] and Peter *et al*. [6] and outlines original articles published from 2011 to 2019. The techniques summarized in this chapter will undoubtedly play a role in many future medical endeavors.

4.2 Capillary electrophoresis of cells

4.2.1 Prokaryotes

A variety of techniques exist for the analysis of microorganisms allowing for their identification and quantitation such as differential staining, serological methods and flow cytometry. However, these procedures require preparation of bacterial cultures, which dramatically lengthens the analysis time [3]. PCR has the advantages of not requiring culture and allowing for higher sensitivity. Yet, sample purification and DNA isolation prior to PCR analysis is slow and complicated [14-15]. Hjertan *et al*. (1987) was the first author reporting the feasibility of moving microbes through capillaries under applied electrical fields [16]. Then, gradually more publications have succeeded, which are well summarized in previous reviews [2-4, 6]. Uncontrolled aggregation of bacterial cells has been stated over the years as a major disadvantage of electrophoretic separations [17-20]. A single peak of high efficiency without multiple peaks attributable to irregular clusters and aggregates of bacterial cells was obtained for the very first time in 2011 by Oukacine *et al*. [21] using ITP with UV detection. An excellent linearity was achieved for *Micrococcus luteus* in the range of 0.4 x 10^8 cells/mL to 2.9 x 10^8 cells/mL. In 2013, Phung *et al*. [22] developed a highly sensitive ITP method with LIF

detection. Cells were stained with the nucleic acid fluorophore SYTO 9 and continuously electrokinetically injected under field amplified (FASI) conditions. Cells were concentrated into a single peak allowing the analysis of *Escherichia coli* with a LOD of 1.35×10^2 cell/mL [22]. Two years later, the same authors reported a counter-pressure-assisted ITP method with electrokinetic injection under FASI conditions to improve the detection of bacterial cells, which improved the LOD for *E. coli* to 78 cells/mL, a factor of 4 when compared with FASI-ITP without counter-pressure [23]. Phung *et al*. also developed a counter-pressure-assisted ITP method in combination with a sieving matrix and ionic spacer to perform in-line fluorescence in situ hybridization (FISH) of bacterial cells. About 50% of the cells injected into the capillary were hybridized with the fluorescently labeled oligonucleotide and separated from the excess unhybridized probe in a two-stage ITP method. The LOD achieved was comparable to the off-line FISH, although the total analysis time was reduced from 2.5 hours to 30 minutes [24]. Dziubakiewicz and Buszewski [25] investigated the behaviour of Gram-positive and Gram-negative bacteria with surface charge modified by calcium ions (Ca^{2+}) under ITP suggesting that Ca^{2+} facilitates overcoming of the electrostatic energy barrier between cells, enabling more compact cell aggregation and electropherograms with a sharp single peak [25].

Many applications of CE techniques have been studied by Horka *et al*. in the last decade, namely for the early stage diagnosis of meningitis. Meningitis is a severe infection of the central nervous system (CNS) that can be caused by bacterial infection. During infection of the CNS, the number of microorganisms in the cerebrospinal fluid (CSF) can range up to hundreds of cells per milliliter. One of the techniques allowing for the analysis of microorganisms is CIEF. However, tens of nanoliters of CSF

injected into the capillary are not enough to determine the real number of pathogens. To overcome this limitation, Horka *et al.* [26] coupled a filtration cartridge with a separation capillary to pre-concentrate the sample, increasing the detection limit by four orders of magnitude. To improve the sensitivity of the detection, 1-[[4-(phenylazo)phenyl]azo]-2- hydroxy-3-naphthoic acid polyethylene glycol ester (PAPAN) was used as dynamic labeling agent for UV/vis detection. Detection sensitivity from 10 to 100 cells/mL of CSF was achieved corresponding to the typical number of microorganisms present in nosocomial CNS infections at early stage. Two years later, CIEF was used by the same group to monitor the concentration of ampholytic antibiotics, such as ampicillin, ciprofloxacin, ofloxacin, tetracycline, tigecycline and vancomycin, in body fluids. The effect of antibiotics on *Staphylococcus epidermidis* during therapy was also determined by CIEF and MALDI-TOF MS as an independent technique to support and confirm data obtained by CIEF. The bacterial fingerprint obtained by MALDI-TOF MS confirmed changes of the examined bacterial cells after their treatment with antibiotics [27]. *Staphylococcus aureus* methicillin-resistant (MRSA) and methicillin susceptible (MSSA) MH-agar cultivated and blood incubated were separated by CZE (**Fig. 4.1**) using a fused silica capillary etched with supercritical water (SCW) and modified with 3-glycidyloxypropyl)trimethoxysilane (GOTMS). This was due to differences in adherence of the MSSA and MRSA cells to the inner surface of the modified fused silica capillary together with the differences in their migration times [28].

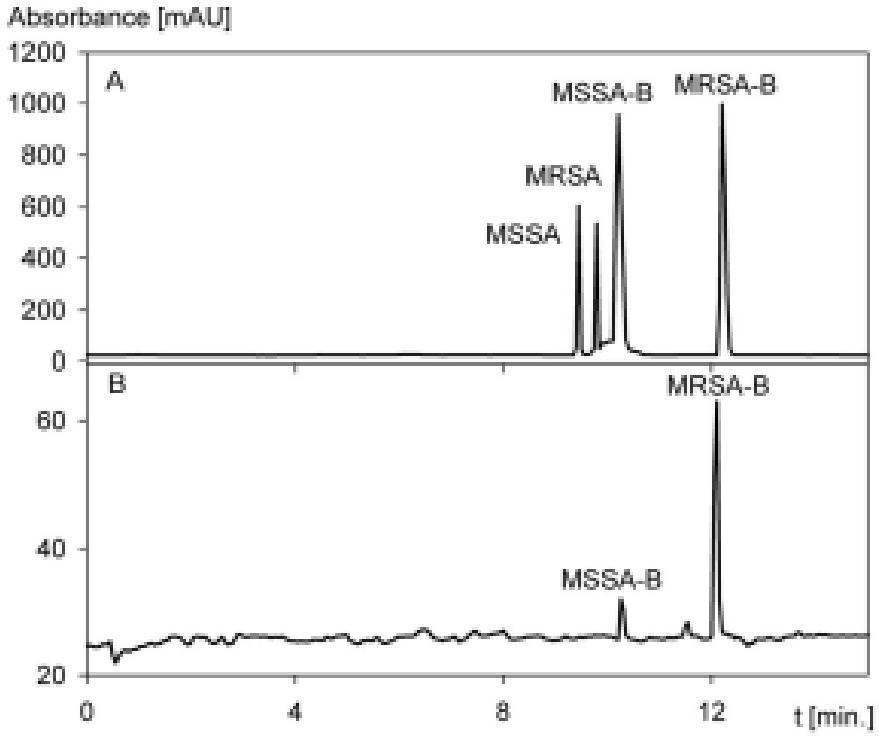

Fig. 4.1 CZE of MSSA and MRSA strains cultivated on (A) MH agar and blood incubated and (B) only blood incubated staphylococci on the etched fused silica capillary modified with GOTMS, syringe pump injection.

Horka *et al*. used the previously developed fused silica capillary etched with SCW and modified GOTMS for the online preconcentration of large-volume sample (0.1- 2.8 μL) of *E. coli* and MRSA and MSSA S. aureus using online combination of transient ITP and MEKC. The hydrodynamic injection of large volumes was possible using a capillary that consisted of two internal diameter segments (input section of 195 μm ID and transition section of 100 μm ID) featuring different inner surface roughness. This novel on-line combination of preconcentration strategies for cells produced up to 680-fold increase in sensitivity for *E. coli* or *S. aureus* cells [29]. To access the number of bacteria in biological samples from patients with postoperative wound infections and understand the impact of antibiotic therapy, Klodzinska and co-workers used CZE. The obtained sensitivity and specificity amounted to 89.5 and 100%, respectively, with

migration time lower than 3.5 min [30]. CZE was also used to study the interaction between Lactobacillus acidophilus, *E. coli* and their protoplasts (bacterial cell whose cell wall has been removed), with single-stranded deoxyribonucleic acid library (ssDNA). The results demonstrated that protoplasts have stronger interaction with ssDNA library than bacteria. *E. coli* was also pretreated by four organic solvents, methanol, ethanol, formaldehyde and glutaraldehyde, to determine the binding efficiency with ssDNA library. Binding constants indicated the interaction of *E. coli* with ssDNA library were in the order: *E. coli* protoplasts > methanol/ethanol treated *E. coli* > formaldehyde/glutaraldehyde treated *E. coli* ≈ *E. coli* not treated. It was suggested that cells surface condition determines their binding affinity with ssDNA [31].

4.2.2 Eukaryotes

CE has been stablished as a powerful tool to analyze subcellular components of mammalian cell extracts and single cell lysates[32-33]. However, there is only a few reports on CE separation of whole mammalian cells presumably because of their susceptibility to lysis due to the absence of an extracellular wall. Yet, the electrophoretic behavior of whole cells has been studied since long using a chamber filled with an electrolyte in which the particles are suspended in free solution. This method was later applied in the capillary format. Wang and Kuo (2014) used CZE to separate neurons derived from induced pluripotent stem cells (iPSCs) and understand the electrical properties of iPSCs based on their electrophoretic mobility during differentiation toward neurons. The results of the study suggested that not only a longer inductive period with nerve growth factor (NGF) produced higher quantity of neuron-like cells, but also high concentration of NGF yielded higher negative charge and a shorter migration time of differentiating iPSCs [34]. This will help controlling the

membrane charge of differentiating iPSCs for future clinical applications. Hirose *et al*. (2017) demonstrated the feasibility of using a CE-based methodology called polymer-enhanced capillary transient isotachophoresis (PectI) to separate a human lung cancer cell line (PC-9) complexed with DNA aptamer candidates from a free randomized DNA library (**Fig 4.2**). The DNA aptamer candidates obtained were proven to bind selectively with high dissociation constant (Kd = 70–350 nM) and form kinetically stable complexes with PC-9 cells [35].

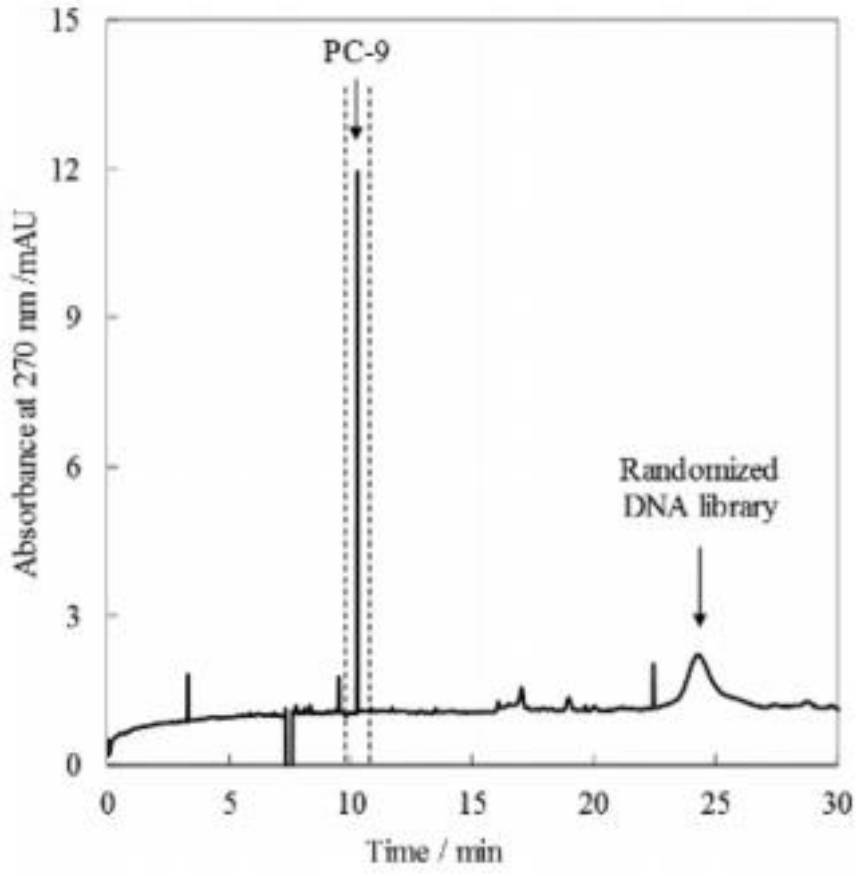

Fig. 4.2 Typical electropherogram of a sample mixture containing PC-9 cells and a randomized ssDNA pool.

Zhang *et al*. developed a system that consisted of an inkjet sampling system, CE system and UV detector (**Fig. 4.3**) for the quantitative separation of normal and

apoptotic HepG2 cells in a mixed cell suspension owing to their electrophoretic mobility differences. The inkjet printer generated droplets containing cells which could be precisely introduced into a capillary. The excellent linearity between the peak area and the droplet number (R^2 = 0.996) indicated that this system enables accurate quantification of cells [36].

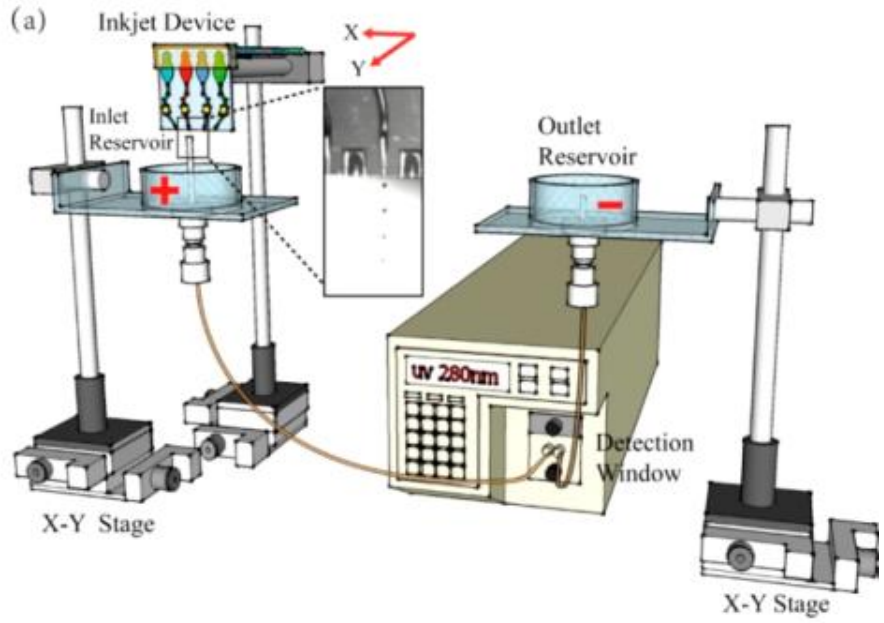

Fig. 4.3 Set up of cell analysis system with capillary electrophoresis. (a) Illustration of homemade equipment. (b) Illustration of inkjet sampling technique with various concentrations of cells. (c) Principle of cells separation in capillary electrophoresis.

4.3 Conclusion

CE has been demonstrated to be suitable for separation of whole bacterial and mammalian cells without too much further optimization. While CE of bacteria is very well stablished and several reviews have been published over two decades, only less than ten original articles can be found on CE of whole mammalian cells. It is anticipated that in the next couple of years CE of mammalian cells will receive more

attention for multiple clinical applications. These developments should encourage microbiologists and cell biologists to use CE to address questions related to their field. Furthermore, the techniques outlined here have a great potential of being transferred to CE microfluidic devices, which are versatile and have high potential on complex sample analysis.

4.4 References

1. Kaiser, C. A.; Krieger, M.; Lodish, H.; Berk, A., *Molecular cell biology*. WH Freeman: 2007.

2. Kenndler, E.; Blaas, D., Capillary electrophoresis of macromolecular biological assemblies: bacteria and viruses. *TrAC, Trends Anal. Chem.* **2001,** *20* (10), 543.

3. Desai, M. J.; Armstrong, D. W., Separation, identification, and characterization of microorganisms by capillary electrophoresis. *Microbiol. Mol. Biol. Rev.* **2003,** *67* (1), 38.

4. Kremser, L.; Blaas, D.; Kenndler, E., Capillary electrophoresis of biological particles: viruses, bacteria, and eukaryotic cells. *Electrophoresis* **2004,** *25* (14), 2282.

5. Subirats, X.; Blaas, D.; Kenndler, E., Recent developments in capillary and chip electrophoresis of bioparticles: Viruses, organelles, and cells. *Electrophoresis* **2011,** *32* (13), 1579.

6. Petr, J.; Maier, V., Analysis of microorganisms by capillary electrophoresis. *TrAC, Trends Anal. Chem.* **2012,** *31*, 9.

7. Jorgenson, J. W.; Lukacs, K. D., Capillary zone electrophoresis. *Science* **1983,** *222*, 266.

8. Quirino, J. P.; Terabe, S., Exceeding 5000-fold concentration of dilute analytes in micellar electrokinetic chromatography. *Science* **1998,** *282* (5388), 465.

9. Rodriguez‐Diaz, R.; Wehr, T.; Zhu, M., Capillary isoelectric focusing. *Electrophoresis* **1997,** *18* (12‐13), 2134.

10. Kaniansky, D.; Marak, J., On-line coupling of capillary isotachophoresis with capillary zone electrophoresis. *J. Chromatogr. A* **1990,** *498*, 191.

11. Malá, Z.; Gebauer, P.; Boček, P., Analytical capillary isotachophoresis after 50 years of development: Recent progress 2014–2016. *Electrophoresis* **2017,** *38* (1), 9.

12. Osbourn, D. M.; Weiss, D. J.; Lunte, C. E., On‐line preconcentration methods for capillary electrophoresis. *ELECTROPHORESIS: An International Journal* **2000,** *21* (14), 2768.

13. Breadmore, M. C.; Grochocki, W.; Kalsoom, U.; Alves, M. N.; Phung, S. C.; Rokh, M. T.; Cabot, J. M.; Ghiasvand, A.; Li, F.; Shallan, A. I., Recent advances in enhancing the sensitivity of electrophoresis and electrochromatography in capillaries and microchips (2016–2018). *Electrophoresis* **2019,** *40* (1), 17.

14. Stinson, S., Identifying bacteria: looking for a fast track. *Chemical & engineering news* **1999,** *77* (13), 36.

15. Tang, Y.-W.; Procop, G. W.; Persing, D. H., Molecular diagnostics of infectious diseases. *Clin. Chem.* **1997,** *43* (11), 2021.

16. Hjerten, S.; Elenbring, K.; Kilár, F.; Liao, J.-L.; Chen, A. J.; Siebert, C. J.; Zhu, M.-D., Carrier-free zone electrophoresis, displacement electrophoresis and isoelectric focusing in a high-performance electrophoresis apparatus. *J. Chromatogr. A* **1987,** *403*, 47.

17. Armstrong, D. W.; Schulte, G.; Schneiderheinze, J. M.; Westenberg, D. J., Separating microbes in the manner of molecules. 1. Capillary electrokinetic approaches. *Anal. Chem.* **1999,** *71* (24), 5465.

18. Armstrong, D. W.; Schneiderheinze, J. M., Rapid identification of the bacterial pathogens responsible for urinary tract infections using direct injection CE. *Anal. Chem.* **2000,** *72* (18), 4474.

19. Schneiderheinze, J.; Armstrong, D.; Schulte, G.; Westenberg, D., High efficiency separation of microbial aggregates using capillary electrophoresis. *FEMS Microbiol. Lett.* **2000,** *189* (1), 39.

20. Armstrong, D. W.; Schneiderheinze, J. M.; Kullman, J. P.; He, L., Rapid CE microbial assays for consumer products that contain active bacteria. *FEMS Microbiol. Lett.* **2001,** *194* (1), 33.

21. Oukacine, F.; Garrelly, L.; Romestand, B.; Goodall, D. M.; Zou, T.; Cottet, H., Focusing and mobilization of bacteria in capillary electrophoresis. *Anal. Chem.* **2011,** *83* (5), 1571.

22. Phung, S. C.; Nai, Y. H.; Powell, S. M.; Macka, M.; Breadmore, M. C., Rapid and sensitive microbial analysis by capillary isotachophoresis with continuous electrokinetic injection under field amplified conditions. *Electrophoresis* **2013,** *34* (11), 1657.

23. Phung, S. C.; Nai, Y. H.; Macka, M.; Powell, S. M.; Guijt, R. M.; Breadmore, M. C., Counter-pressure-assisted ITP with electrokinetic injection under field-amplified conditions for bacterial analysis. *Analytical and bioanalytical chemistry* **2015,** *407* (23), 6995.

24. Phung, S. C.; Cabot, J. M.; Macka, M.; Powell, S. M.; Guijt, R. M.; Breadmore, M., Isotachophoretic fluorescence in situ hybridization of intact bacterial cells. *Anal. Chem.* **2017,** *89* (12), 6513.

25. Dziubakiewicz, E.; Buszewski, B., Capillary electrophoresis of microbial aggregates. *Electrophoresis* **2014,** *35* (8), 1160.

26. Horká, M.; Růžička, F.; Kubesová, A.; Šlais, K., Dynamic labeling of diagnostically significant microbial cells in cerebrospinal fluid by red chromophoric non-ionogenic surfactant for capillary electrophoresis separations. *Anal. Chim. Acta* **2012,** *728,* 86.

27. Horká, M.; Vykydalová, M.; Růžička, F.; Šalplachta, J.; Holá, V.; Dvořáčková, M.; Kubesová, A.; Šlais, K., CIEF separation, UV detection, and quantification of ampholytic antibiotics and bacteria from different matrices. *Anal. Bioanal. Chem.* **2014,** *406* (25), 6285.

28. Horka, M.; Tesarova, M.; Karasek, P.; Ruzicka, F.; Hola, V.; Sittova, M.; Roth, M., Determination of methicillin-resistant and methicillin-susceptible Staphylococcus aureus bacteria in blood by capillary zone electrophoresis. *Anal. Chim. Acta* **2015,** *868,* 67.

29. Horká, M.; Karásek, P.; Roth, M.; Růžička, F., Pre-concentration and separation of bacteria by volume coupling electrophoresis on supercritical water-etched fused silica capillary with two segments of different internal diameters and inner surface roughnesses. *Anal. Bioanal. Chem.* **2018,** *410* (1), 167.

30. Kłodzińska, E.; Jaworski, M.; Kupczyk, W.; Jackowski, M.; Buszewski, B., A study of interactions between bacteria and antibiotics by capillary electrophoresis. *Electrophoresis* **2012,** *33* (19-20), 3095.

31. Meng, C.; Zhao, X.; Qu, F.; Mei, F.; Gu, L., Interaction evaluation of bacteria and protoplasts with single-stranded deoxyribonucleic acid library based on capillary electrophoresis. *J. Chromatogr. A* **2014,** *1358*, 269.

32. Woods, L. A.; Roddy, T. P.; Ewing, A. G., Capillary electrophoresis of single mammalian cells. *Electrophoresis* **2004,** *25* (9), 1181.

33. Stuart, J. N.; Sweedler, J. V., Single-cell analysis by capillary electrophoresis. *Anal. Bioanal. Chem.* **2003,** *375* (1), 28.

34. Wang, C.-C.; Kuo, Y.-C., Capillary electrophoresis of induced pluripotent stem cells during differentiation toward neurons. *Journal of the Taiwan Institute of Chemical Engineers* **2014,** *45* (5), 2096.

35. Hirose, K.; Tsuchida, M.; Asakura, H.; Wakui, K.; Yoshimoto, K.; Iida, K.; Sato, M.; Shibukawa, M.; Suganuma, M.; Saito, S., A single-round selection of selective DNA aptamers for mammalian cells by polymer-enhanced capillary transient isotachophoresis. *Analyst* **2017,** *142* (21), 4030.

36. Zhang, W.; Li, N.; Zeng, H.; Nakajima, H.; Lin, J.-M.; Uchiyama, K., Inkjet Printing Based Separation of Mammalian Cells by Capillary Electrophoresis. *Anal. Chem.* **2017,** *89* (17), 8674.

Chapter 5. Isotachophoresis of Functionalised Magnetic Nanoparticles and Quantum Dots for Studies on Cell Uptake

Abstract

Isotachophoresis (ITP) is a robust electrokinetic technique that can achieve million-fold preconcentration and efficient separation based on ionic mobility. It was also recently shown to provide exceptional improvements in the hybridization reaction rate between nucleic acids and antibody and antigens. In this chapter, carboxylic acid functionalized iron oxide nanoparticles and carboxylic acid functionalised quantum dots were focused with *Escherichia coli* TOP10 cells at the same isotachophoretic boundary to investigate their electrostatic adsorption to the cell wall and their cellular uptake. ITP-labelling of bacterial cells with iron oxide nanoparticles may provide all kinds of cells with sufficient magnetization in less than 5 minutes to allow cell detection by high-resolution magnetic resonance imaging (MRI) and to enable magnetic manipulation. Similarly, quantum dots can be interesting fluorescent probes due to their reduced tendency to photobleach and potential usage for tracking the path and the fate of individual cells.

5.1 Introduction

Cell labelling in living organisms is a topic of interest due to its various biological and medical applications. To facilitate cell labelling, different strategies have been developed. The first class of strategies consist of labelling cell surface receptors to

detect specific cells of interest. The second class, currently chosen in most of cell imaging assays, involves the use of a transfection agents that help the internalization of molecular probes. Due to the non-specificity of this method, it can be applied to a wide variety of cells.

Highly charged electrostatic interactions between nanoparticles and cells have been demonstrated to induce membrane adsorption and intracellular uptake in particular conditions [1-2] in similar way to the conventionally used strategies to introduce nucleic acids into cells. Phung *et al*. used isotachophoresis (ITP) to accelerate the transport of oligonucleotides into bacterial cells by fluorescence in situ hybridisation (FISH) for cell enumeration [3]. In this chapter, the ITP of carboxylic acid functionalised magnetic nanoparticles (MNP-COOH) and carboxylic acid functionalised quantum dots (QD-COOH) has been shown and their potential use for internalisation and labelling of cells has been investigated.

5.2 Experimental

5.2.1 Reagents

Commercial iron oxide nanoparticles Fe_3O_4 (ca. 11 nm), high purity, 99.5+% were purchased from US Research Nanomaterials, Inc., iron oxide nanoparticles with carboxylic acid groups in deionised water were purchased from Ocean NanoTech LLC (ca. 10 nm) and CdSeS/ZnS alloyed quantum dots COOH functionalised, fluorescence λ_{em} 490 n, 6 nm diameter, 1 mg/mL in water were purchased from Sigma-Aldrich. Tris(hydroxymethyl)aminomethane (Tris) ≥99.9%, tetramethylammonium hydroxide ≥97%, polyvinylpyrrolidone (PVP), 4-(2-hydroxyethyl)-1 piperazineethanesulfonic acid (HEPES) 99.5% and dimethyl sulfoxide anhydrous (DMSO) ≥ 99.9% were

purchased from Sigma-Aldrich. Phosphate-buffered (PBS) was purchased from Oxoid. Milli-Q Millipore Gradient System was used for all the solutions preparation.

5.2.2 Capillary electrophoresis

All CE experiments were carried out on a Beckman Coulter P/ACE MDQ Capillary Electrophoresis System equipped with a UV detector with acquisition enabled at 280 nm (for analysis of bare MNPs and MNP-COOH) and a Beckman Coulter P/ACE MDQ Capillary Electrophoresis System equipped with a 488-nm laser module (for analysis of QD-COOH). Experiments were conducted using a bare fused silica capillary (Polymicro Technology, AZ, USA) of 50 µm id with total length of 40 cm (30 cm effective length to detector).

5.2.3 Capillary conditioning

Prior to use, the new capillaries were pre-conditioned at 20 psi in the following order: 1 M NaOH (30 min), Milli-Q water (20 min), 1 M HCl (20 min), Milli-Q water (10 min) followed by 1 % w/v PVP at 45 psi for 45 min. Finally, the capillary was conditioned with LE at - 16 kV for 10 min.

5.2.4 Electrolytes

The composition for the leading electrolyte (LE) was 10 mM Tris-nitrate, 20 mM TMAOH, 0.5% (w/v) PVP, pH 7.9. The composition for the terminating electrolyte (TE) was 10 mM Tris-HEPES, 20 mM TMAOH, 0.5% (w/v) PVP, pH 7.9. The electrolytes were prepared using 18.2 Milli-Q water.

5.2.5 Isotachophoresis

Each analysis began by flushing the capillary with LE solution for 3 min at 20 psi and continuous electrokinetic injection of bare MNP/MNP-COOH/ MNP-COOH and *E. coli* TOP10/QD-COOH/ QD-COOH and *E. coli* TOP10 suspended in TE at -16 kV. For ITP with counter pressure, simultaneous application of voltage (-16 kV) and counter-pressure (1.3 psi) was made for 20 min. The counter pressure was then removed to allow analytes passing though the detector.

5.3 Results and discussion

Initially, bare superparamagnetic magnetite nanoparticles (BSPMNPs) were subjected to ITP using 10 mM Tris-nitrate, 20 mM TMAOH, 0.5% (w/v) PVP, pH 7.9 as LE. The TE was composed of the same cation (Tris) and HEPES was chosen as the terminating anion for having lower electrophoretic mobility than BSPMNPs. The additive TMAOH was part of the electrolyte composition for its demonstrated capability of electrostatically stabilize BSPMNPs [4]. However, more than one peak was present in electropherograms indicative of nanoparticle clusters (**Fig 5.1**) induced by ITP focusing. In contrast, a single peak of MNP-COOH at the LE/TE interface was observed under the same separation conditions. To test the feasibility of using ITP for internalization and labelling cells, MNP-COOH (15 nm diameter) and *E. coli* TOP10 were focused at the same boundary. To extend the contact time between *E. coli* TOP10 and MNP-COOH, a counter pressure that opposes the voltage induced ITP movement was applied for 20 minutes to hold the MNP-COOH and *E. coli* TOP10 cells into the capillary (**Fig 5.2**).

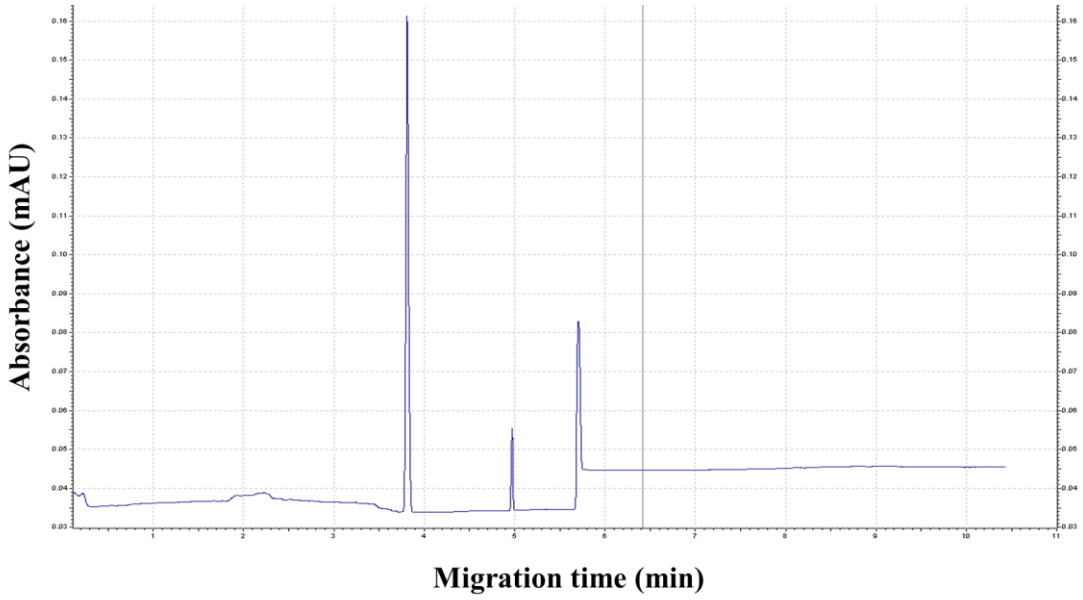

Fig. 5.1 Isotachopherogram of 10.0 µg bare MNP.

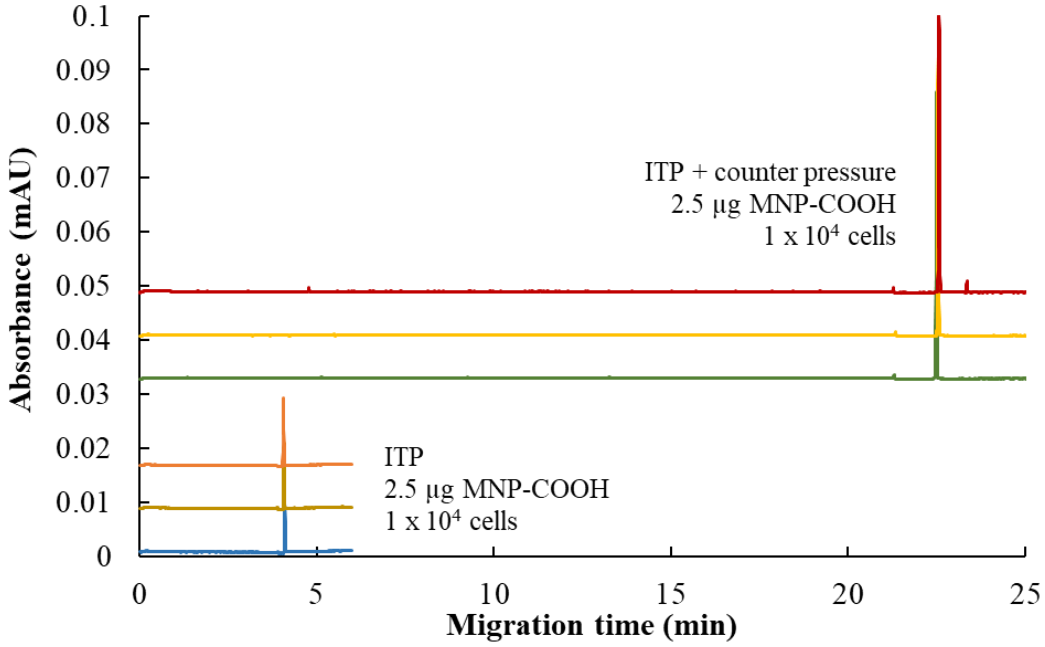

Fig. 5.2 Triplicates of isotachopherograms of a mixture of 2.5 µg and 1 x 10^4 with and without application of counter pressure cells.

After each ITP run, *E. coli* TOP10 cells were collected from the outlet vial, immediately transferred into ice, and 100 µL of S.O.C. medium was added. The cells were then incubated for 3 hours at 37 °C in 2 mL CE vials, which were firmly

positioned on the top of a strong magnetic strip. To determine how many cells incorporated magnetic nanoparticles, cell suspensions were washed 5 times with 100 µL of PBS. The autosampler CE vials were maintained in contact with the strong magnetic strip until the last wash. A volume of 100 µL was spread on pre-warmed LB agar plates and incubated overnight at 37 °C. The cells incorporating or attaching MNP-COOH were determined by plate counting. The results are shown in **Fig 5.3**.

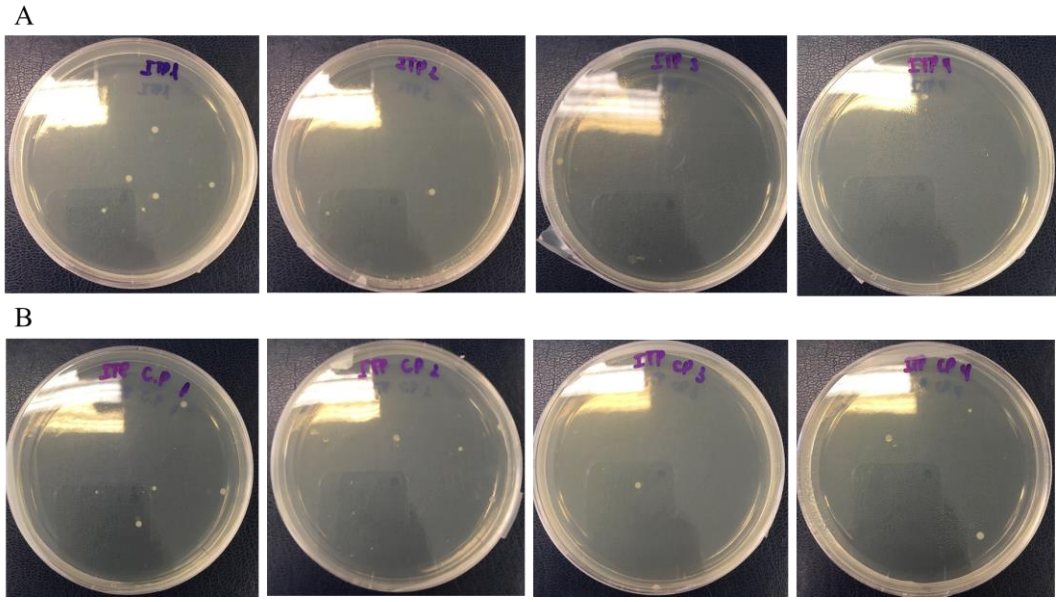

Fig. 5.3 Replicates (n=4) of *E. coli* TOP10 cells collected from the outlet vial after ITP focusing with MNP-COOH grown in LB agar plates incubated overnight at 37 °C. (A) without counter pressure, (B) with counter pressure.

It was observed TOP10 colonies in all the quadruplicated experiments at 2.5 ± 2.1 and 5.3±4.0 CFU without and with counter-pressure, respectively. The CFU count between both modes was not statistically different, but the presence of colonies was indicative of MNP-COOH incorporation or attachment to the *E. coli* TOP10 cells surface during ITP focusing. To increase the sensitivity of this method and reduce the assay time, ITP focusing of QD-COOH (10 nm diameter) and *E. coli* TOP10 cells was

performed (**Fig. 5.4**). The cells were subsequently recovered and washed 5 times using centrifugation and directly visualised by fluorescence microscopy. This method could save over 16 hours compared to the method for MNP-COOH by eliminating an overnight incubation step. However, no fluorescent cells were visualised, which can relate to their small size and/or limited resolution of the fluorescence microscope used.

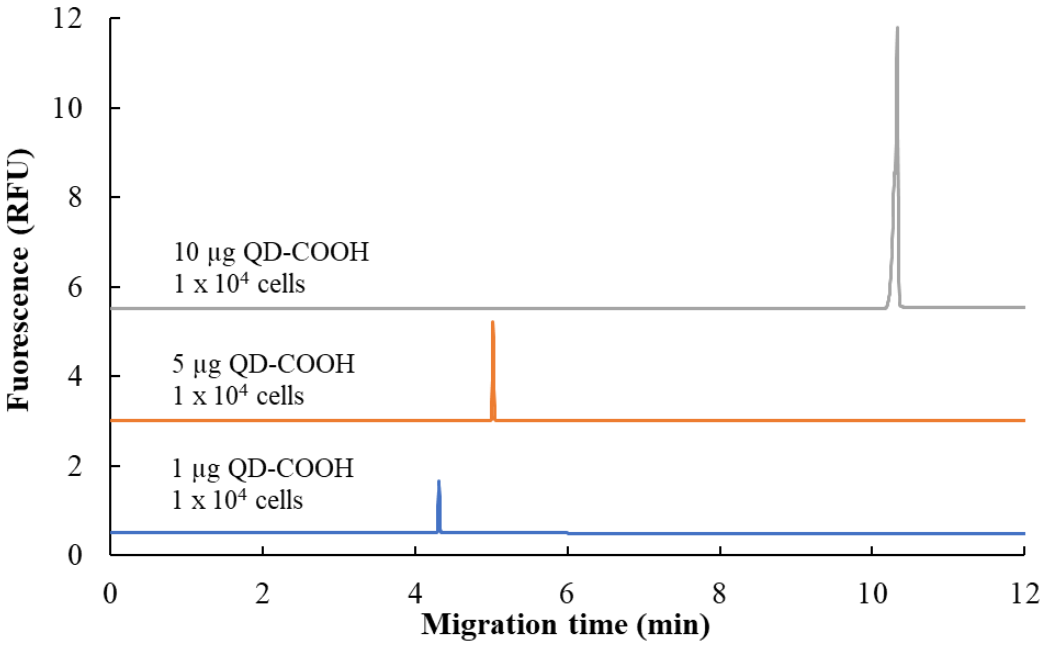

Fig. 5.4 Isotachopherograms of *E. coli* TOP10 cells and QD-COOH focused at the same LE/TE interface.

5.4 Conclusion

In this chapter we show the ITP of MNP-COOH (ca. 10 nm) and QD-COOH (ca. 10 nm) and investigate their potential use for internalisation and labelling of cells. This labelling method can be applied in a very simple way without modification of nanoparticles surface, it is rapid and applicable for every kind of cell. To have a clear understanding of the efficiency of ITP in cell uptake/interaction of /with: (a) MNP-COOH, more sensitive techniques for magnetic detection should be applied such as

giant magnetoresistance (GMR), nuclear magnetic resonance (NMR) and superconducting quantum interference devices (SQUID); (b) QD-COOH, a more robust fluorescence microscope should be used, or flow cytometry as an alternative.

5.5 References

1. Wilhelm, C.; Gazeau, F., Universal cell labelling with anionic magnetic nanoparticles. *Biomaterials* **2008,** *29* (22), 3161.

2. Becker, C.; Hodenius, M.; Blendinger, G.; Sechi, A.; Hieronymus, T.; Müller-Schulte, D.; Schmitz-Rode, T.; Zenke, M., Uptake of magnetic nanoparticles into cells for cell tracking. *J. Magn. Magn. Mater.* **2007,** *311* (1), 234.

3. Phung, S. C.; Cabot, J. M.; Macka, M.; Powell, S. M.; Guijt, R. M.; Breadmore, M., Isotachophoretic fluorescence in situ hybridization of intact bacterial cells. *Anal. Chem.* **2017,** *89* (12), 6513.

4. Alves, M. N.; Nesterenko, P. N.; Paull, B.; Haddad, P. R.; Macka, M., Separation of superparamagnetic magnetite nanoparticles by capillary zone electrophoresis using non‐complexing and complexing electrolyte anions and tetramethylammonium as dispersing additive. *Electrophoresis* **2018,** *39* (12), 1429.

Chapter 6. Isotachophoresis for Rapid Transformation of *Escherichia coli*

Chapter 6 has been removed for copyright or proprietary reasons.

*The research contained in this chapter has been filed for patent protection as M.N. Alves, M.C. Breadmore, Y.H. Nai, S. Powell, M. Macka, Isotachophoretic nucleic acid transformation of cells, Australian Provisional Patent Application No AU2019902240, Filed 26/6/2019.

Chapter 7. Isotachophoresis and its Applicability to Transfection of Mammalian Cells

Abstract

A simple procedure for the introduction of plasmid DNA into $5x10^3$ mammalian cells by isotachophoresis is described. Plasmid DNA and Jurkat cells are sequentially injected into a Rtx wax (fused silica) capillary with 60 cm total length and 100 µm ID and focused into 19 nL by isotachophoresis induced by application of constant voltage (3 kV). Jurkat cells were purposely selected since it transfects poorly under electroporation, offering frequencies which are sometimes insufficient for their practical applications. Through this method, Jurkat cells were transfected at higher rate than electroporation, using a completely new approach that, unlike electroporation, can be easily automated and allow for high sample processing throughput.

7.1 Introduction

The transfection of DNA and the delivery of cell membrane impermeable biomolecules into mammalian cells are among the most important research tools in modern molecular biology. Many methods have been developed to introduce foreign material into mammalian cells. The most commonly applied methods are electroporation, calcium phosphate co-precipitation, lipofection and viral vectors. Recently, magnetofection, optoporation and sonoporation have also emerged as powerful and efficient techniques for cell transfection[1-3]. The transfection efficiency by these methods varies considerably among different cell lines and may be unacceptably low in many cases. This may pose difficulties in experiments that depend

on the use of specific cell lines corresponding to a given tissue type. Therefore, there is a great need for methods that can introduce DNA into mammalian cells with high efficiency and without restriction to cell type.

ITP is a robust and powerful electrokinetic technique based on ionic mobility that can attain 1,000,000-fold online preconcentration [4]. Recent studies have shown that ITP has wider applications, namely, to enhance hybridization rate of nucleic acid in free solution. Phung *et al*. utilized ITP to accelerate the intracellular transport of oligonucleotides into intact bacterial cells for in-line fluorescence in vitro hybridization (FISH) [5] and in Chapter 6, ITP was used to introduce plasmid DNA into Escherichia coli TOP10. The transformation rate achieved for *E. coli* TOP10 was 1,000-fold superior to conventional methods at survival rates higher than 60%. To investigate the feasibility of ITP to introduce plasmid DNA into different cell types, here, Jurkat cells (human T-lymphocyte; acute T-cell leukemia cell line) were used and the expression of GFP was measured as an indicator of transfection efficiency. Jurkat cells were selected due to their inherent difficulty of being transfected. The conditions most conducive to high cell viability were investigated in order to obtain the maximum number of transfectants. The efficiency of ITP transfection under optimal conditions was compared to that obtained using electroporation.

7.2 Experimental

7.2.1 Jurkat cells preparation

Jurkat cells were cultured in RPMI1640 medium (Gibco) supplemented with 10% fetal bovine serum (FBS; Gibco). Cells were cultured in a humidified incubator at 37 °C with 5% CO^2 and passaged every 2 days. In the second day, cells at late log growth

phase were harvested by gentle centrifugation for 8 min at 250 x g at 4°C and resuspended in TE to a final concentration of 9-10 x 10^6 cells/mL.

7.2.2 Capillary electrophoresis

All CE experiments were carried out on a Beckman Coulter P/ACE MDQ CE system equipped with a UV detector with acquisition enabled at 280 nm. The capillary temperature was maintained at 25°C. Experiments were conducted using a Rtx Wax GC column (fused silica) of 100 µm id with total length of 60 cm (50 cm effective length to detector). UV detection was utilized for the validation of the ITP method. The UV detector was turned off for ITP transfections.

7.2.3 Electrolytes

For all ITP experiments, the LE used was 0.60 M sodium-phosphate (pH 7.3) and the TE was 0.60 M sodium-HEPES (pH 7.3). The electrolytes were prepared using 18.2 MΩ cm-1 Type I purified water (Milli-Q®, Millipore, Bedford, MA, USA). The electrolytes were subsequently filtered through a sterile 0.22 µm syringe filter (Millex-GS Merck, Australia).

7.2.4 ITP transfection

Each analysis began by filling the capillary with LE for 3 min at 20 psi, hydrodynamic injection of DNA (in LE) at 5 psi for 5 seconds (0.19 µg plasmid DNA), hydrodynamic injection of Jurkat cells in TE at 5 psi for 10 seconds (5 x 10^3 cells), and application of 3 kV between the inlet (TE) and outlet (LE) vials.

7.2.5 ITP transfection success

After each run, the Jurkat cells collected in the outlet vials were immediately transferred to ice and 3 mL of non-selective medium was added. After 16 hours, the medium was supplemented with Penicillin-Streptomycin (Gicbo). Protein (GFP) expression was assayed 48 hours after the ITP transfection. The Jurkat cells are observed by fluorescence microscopy and counted in a hemocytometer The transformation efficiency was calculated dividing the number GFP positive cells by the amount of plasmid DNA injected. The transformation rate was calculated based on the percentage of individual cells capable of being transformed.

7.2.6 Preparation of Jurkat cells for electroporation

Late log phase cell cultures were harvested by centrifuging 7 minutes at 250 x g, 4 °C. Cells were resuspended in ice-cold TE to a cell concentration of 9-10 x 10^6 and diluted 600 times for the EP of 10^3 cells. Aliquots of 0.4 mL of cell suspension were transferred into cuvettes (0.4 cm gap width) set on ice and incubate 5 min on ice. Plasmid DNA (0.19 µg) was added in cuvettes on ice. These were connected to a power supply, and the cells subjected to a high voltage electrical pulse of 0.2 kV. The cells were then allowed to recover briefly by returning them to ice for 10 min before being placed in non-selective cell growth medium.

7.3 Results and discussion

Based on the ITP conditions reported in the previous chapter for the rapid transformation of *E. coli* TOP10, initially 0.05 M Tris-HCl (pH 7.9) was selected as LE and 0.05 M Tris-HEPES (pH 7.9) as TE for the ITP of Jurkat cells. However, the ITP focusing of Jurkat T cells using this buffer composition was found unsuccessful.

Subsequently, cell viability was monitored for 1 hour by suspending Jurkat cells in 0.05 M Tris-HCl (pH 7.9) and 0.05 M Tris-HEPES (pH 7.9). It was clearly noticeable that most cells were lysed after a few minutes. Lysed cells were not seen under the microscope or appeared as debris/cell fragments [i.e. lysed cells = initial cells - (live cells + dead cells)]. It was suspected that cell lysis caused less intact cells (live and dead) being ITP focused, which were not detectable by UV at 280 nm, perhaps due to the poor sensitivity of the detector. Therefore, a new buffer composition was formulated containing dominant ionic species of phosphate buffer saline (PBS): sodium and phosphate. The 0.16 M sodium-phosphate (pH 7.3) was chosen as LE and 0.16 M sodium-HEPES (pH 7.3) as TE, such that the anion phosphate and the anion HEPES have higher and lower effective electrophoretic mobilities than the Jurkat cells, respectively. This allows the cells with an intermediate effective electrophoretic mobility to concentrate and focus at the moving LE-TE interface. To evaluate the cell viability, damaged cells were identified with trypan blue staining. Cell viability was expressed as percentage of non-stained cells relative to the total number of cells in the analysed visual field of a hemocytometer. The viability of Jurkat cells incubated in 0.16 M sodium-phosphate (pH 7.3) and 0.16 M sodium-HEPES (pH 7.3) was above 80% for more than 10 hours, which was comparable to the viability of cells incubated in culture medium or PBS (**Fig 7.1**). Dimethyl sulfoxide (DMSO) was further incorporated in the TE since it is a well-established cell-penetrating enhancer for intracellular delivery. A concentration of 0.1% (v/v) DMSO was chosen since it did not affect the viability of Jurkat cells neither attach to the capillary wall interfering with the ITP focusing. The importance of having DMSO present at the ITP interface for Jurkat cell transfection is still discussable because DMSO is neutral and if there is

a residual EOF from LE towards TE, it is expected DMSO to simply stay in the TE and never propagate with/to the ITP interface.

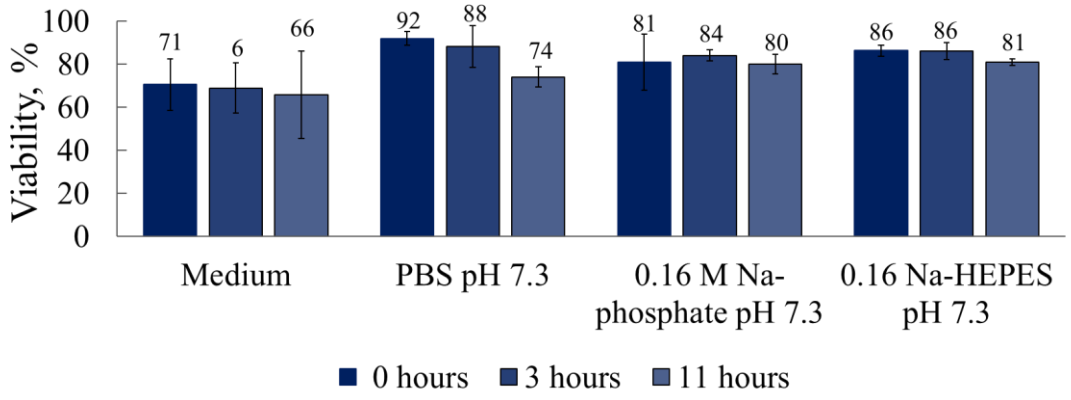

Fig.7.1 Viability of Jurkat cells over incubation time in medium, PBS (pH 7.3), sodium-phosphate (pH 7.3) and sodium-HEPES (pH 7.3). Average and SD calculated based on 4 replicates of Jurkat cells suspended and incubated in media and 3 types of buffers (PBS, 0.16 M Na-phosphate, and 0.16 M Na-HEPES) for 0, 3 and 11 hours.

Negatively charged encapsulated fluorescent beads with mean size of 0.51 μm were previously used as a model analyte for bacterial analysis as their size is similar to that of *E. coli* [6]. Similarly, here, negatively charged fluorescent carboxyl-functionalised microspheres with mean diameter of 0.51 μm and 15.45 μm were used as model to predict the approximate migration time of Jurkat cells, which have an intermediate diameter of ca. 10 μm. In lieu of an untreated fused silica capillary, ITP was performed using a Rtx Wax GC column (fused silica) with cross bond polyethylene glycol (PEG) to supress the electroosmotic flow (EOF). Thus, new capillaries were not required to be conditioned as previously (see Chapter 6 section 6.2.4), saving 2 hours' time and allowing the use of less complex electrolytes. It was inferred that at field strength of 0.075 kV/cm (3 kV) in a 40 cm x 100 μm ID Rtx Wax GC column (fused silica), Jurkat

cells are eluted in less than 35 min (data not shown). For the ITP transfection, late-log phase 9-10 x 10^6 cells/mL were placed in the inlet vial. To yield a reasonable number of transfectants, the length of the capillary was increased from 40 to 60 cm and hydrodynamic injections were performed to monitor the amount of DNA and cells used per reaction. Transfected cells were observed when 0.19 µg plasmid and 5 x 10^3 cells were injected. The ITP method developed consisted of filling the capillary with LE, followed by individual hydrodynamic injections DNA (suspended in LE) and cells (suspended in TE) in this order, and finally, the inlet vial is switched to TE. When the voltage is applied, an electric field gradient is created at the ITP interface causing plasmid DNA and Jurkat cells to be concentrated and focused in a small volume at the moving ITP interface (ca 2.4 mm section of the capillary corresponding to ca 19 nL). The validation of the ITP method is represented in **Fig. 7.2A** showing the focusing of plasmid and cells within the same peak at the ITP interface at 116 min in the electropherogram. At the ITP interface, cells experience an electric field (ca 0.05 kV.cm-1) that induces the uptake of plasmid DNA from the surrounding medium presumably through the formation of transient pores in the cell membrane. The cells are finally collected from the outlet vial and cultured in 3 mL of non-selective medium. After 16 hours, penicillin-streptomycin is added to prevent bacterial contamination of the Jurkat cells culture due to their effective combined action against gram-positive and gram-negative bacteria. Protein (GFP) expression is assayed 48 hours post ITP transfection, the transfection rate and efficiency are examined by fluorescence microscopy (**Fig 7.2B**) and the cell count was performed using a hemocytometer.

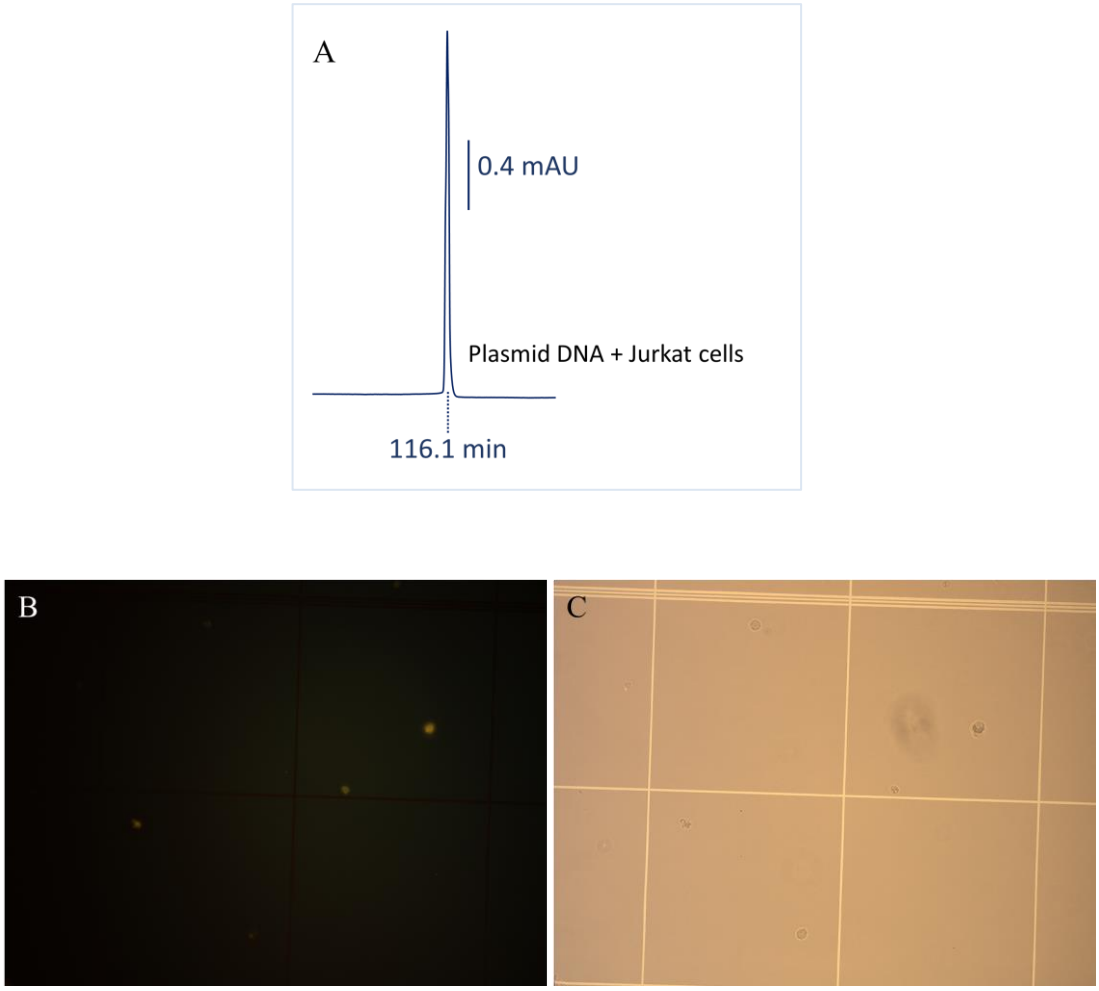

Fig. 7.2 ITP transfection of Jurkat cells. (A) Validation of the ITP method showing the focusing of plasmid and cells within the same peak at the ITP interface. (B) Protein (GFP) expression assayed 48 hours after ITP transfection by fluorescence microscopy and (C) phase-contrast microscopy.

The transfection of Jurkat cells with the mammalian vector pCMV6-AC-GFP (high copy number, codifying for GFP, 6.6 kb) via ITP and EP were compared in terms of transfection rate (percentage of cells that were transformed) and transfection efficiency (efficiency of DNA uptake i.e. transfected cells/µg DNA). The ITP transfection of Jurkat cells with the mammalian vector pCMV6-Entry (high copy number, not codifying for GFP, 4.9 kb) was used as negative control.

A suspension of about 9-10 x 10^6 cells/mL was initially prepared for EP, which was subsequentially diluted 600-fold for the EP of low cell number. For EP, a volume of 0.4 mL cell suspension was placed in 0.4 cm-gap EP cuvettes. The ITP transfection was performed by placing the suspension of 9-10 x 10^6 cells/mL in the inlet vial of a Beckman Coulter P/ACE MDQ CE system. A hydrodynamic injection of 5 psi for 10 seconds allowed injections of about 5 x 10^3 cells. The live/dead cells were quantified before EP transfection. For the ITP transfection, the initial live/dead cells were estimated based on the initial live/dead counts in the 9-10 x 10^6 cells/mL suspension. The results demonstrated that the transfection efficiency obtained by EP of 10^6 cells (9.18 x 10^6 cell/µg DNA) (**Fig. 7.3A**) was ca 400-fold higher than the transfection efficiency obtained using 10^3 cells via EP (2.18 x 10^4 cell/µg DNA) (**Fig. 7.3B**). The GFP positive cells obtained from ITP transfection are shown in figure **Fig. 7.3C.** The average transfection efficiency through ITP (2.42 x 10^4 cell/µg DNA) was slightly higher than the average transfection efficiency achieved via EP of 10^3 cells, but not significantly different (**Fig. 7.3E**). In contrast, the transfection rate was about 40% higher for ITP transfection compared to EP of 10^6 and 10^3 cells (**Fig. 7.2D**). These results significantly differed from EP of 10^6 cells but not from EP of 10^3 cells.

An explanation for the higher number of GFP positive cells achieved by ITP may be related to lower cell death in presence of an electric field of 0.05 kV.cm-1 vs. 0.75 kV.cm-1. However, it could not be proven because of the limited sensitivity of the hemocytometer. It can also result from a large excess of DNA molecules over the cells (5.22 x 10^6:1) at the ITP interface. The high standard deviations obtained throughout the transfection experiments is result of the low cell number in the counting field of the hemocytometer. This phenomemum was difficult to avoid due to the limited

number of cells injected into the capillary. The capillary dimensions selected resulted from a compromise between the duration of the transfection event (the extension of the capillary length drastically increased the migration time of Jurkat cells and DNA) and Joule heating (greater capillary radius compromised cell viability due to higher heat release).

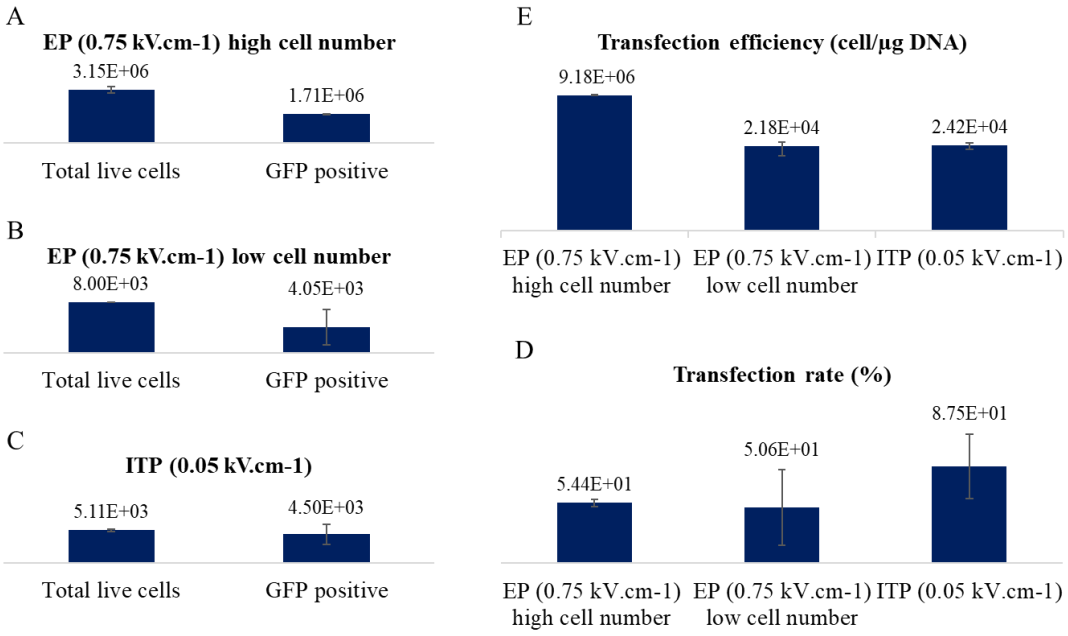

Fig. 7.3 GFP positive cells obtained via EP transfection of (A) 10^6 and (B) 10^3 cells; GFP positive cells obtained via ITP transfection of 10^3 cells (C). Transfection rates (D) achieved by EP (10^6 and 10^3 cells) and ITP (10^3 cells), and transfection efficiency (E) achieved by EP (10^6 and 10^3 cells) and ITP (10^3 cells). Average and SD based on 4 replicates of EP high cell number (10^6 cells), 4 replicates of EP low cell number (10^3 cells) and 4 replicates of ITP of 10^3 cells.

Overall, this study has proven that ITP transfection of Jurkat cells with pCMV6-AC-GFP is an approach with comparable robustness to EP. ITP transfection is a versatile technique with demonstrated applicability to prokaryotic or eukaryotic cells, it is efficient, requires low amount of DNA and can operate in living organisms.

7.4 Conclusion

The ITP transfection here described is simple and highly efficient. It only requires two electrolytes (sodium-phosphate and sodium-HEPES), application of constant voltage (3kV), 5 x 10^3 cells and 0.19 µg of plasmid DNA. Through this method, Jurkat cells were transfected at a rate of 88% with the vector pCMV6-AC-GFP, while EP of 10^6 and 10^3 cells only achieved 54% and 51%, respectively. The fact that both procedures involve the physical interaction between an electric field and the cell membrane, make them less dependent on cell type than other methods. However, ITP transfection is suitable for handling large sample sets when organized in 96-well plates adapted to a multichannel capillary electrophoresis device, which increases automation and sample processing throughput. This method appears as a supplement to the existing arsenal of methods for obtaining cellular expression of sequence information present on molecules of exogenous DNA without requiring complicated cell purification procedures and with no issues related to biosafety and mutagenesis as viral vectors do. The transfection success of ITP transfection encourages the application of this method as a newly emerging attractive option for recombinant protein production.

7.5 References

1. Scherer, F.; Anton, M.; Schillinger, U.; Henke, J.; Bergemann, C.; Krüger, A.; Gänsbacher, B.; Plank, C., Magnetofection: enhancing and targeting gene delivery by magnetic force in vitro and in vivo. *Gene therapy* **2002,** *9* (2), 102.

2. Schneckenburger, H.; Hendinger, A.; Sailer, R.; Strauss, W. S.; Lyttek, M.; Schmitt, M., Laser-assisted optoporation of single cells. *Journal of biomedical optics* **2002,** *7* (3), 410.

3. Miller, D. L.; Pislaru, S. V.; Greenleaf, J. F., Sonoporation: mechanical DNA delivery by ultrasonic cavitation. *Somatic cell and molecular genetics* **2002,** *27* (1-6), 115.

4. Jung, B.; Bharadwaj, R.; Santiago, J. G., On-chip millionfold sample stacking using transient isotachophoresis. *Anal. Chem.* **2006,** *78* (7), 2319.

5. Phung, S. C.; Cabot, J. M.; Macka, M.; Powell, S. M.; Guijt, R. M.; Breadmore, M. C., Isotachophoretic Fluorescence in situ Hybridization of intact bacterial cells. *Anal. Chem.* **2017,** *89*, 6513.

6. Phung, S. C.; Nai, Y. H.; Macka, M.; Powell, S. M.; Guijt, R. M.; Breadmore, M. C., Counter-pressure-assisted ITP with electrokinetic injection under field-amplified conditions for bacterial analysis. *Anal. Bioanal. Chem.* **2015,** *407* (23), 6995.

Chapter 8. Conclusions and future work

The improvement of the existing approaches of synthetizing uniform and more monodisperse M(N)Ps has been notorious in recent years. However, even the most efficient and highly optimized protocols yield samples relatively polydisperse. This is an obstacle to some emerging applications of M(N)Ps with some specific functions, particularly in biomedical areas as their properties are dependent. Analytical tools are fundamental to understand the behaviour of MNPs according to their size, shape and surface chemistry. This knowledge can give information on the monodispersity and purity of M(N)Ps for their ultimate practical use. A strategy for BSPMNPs separations has been reported based on CE using rationally formulated electrolyte compositions. For the first time, symmetrical and smooth peaks of BSPMNPs were observed in electropherograms free of spurious spikes otherwise typical of CE separations and characteristic of nanoparticle clusters. This was achieved through electrostatic stabilization of BSPMNPs using an electrolyte composed of Tris-citrate, sodium phosphate and the additive TMAOH. Although TMAOH has been used for more than two decades in the synthesis of well dispersed magnetite nanoparticle colloidal solutions, we have demonstrated its utility for effective CE separations of dispersed BSPMNPs and for better understanding of their surface chemistry. Using Tris-nitrate containing 20 mM of TMAOH as electrolyte, the separation of BSPMNPs and carboxylic acid functionalized iron oxide nanoparticles was also made possible. Our findings show that new formulations and designs of modified nanoparticles for numerous applications can be monitored and characterized based on simple and rapid CE experiments. After the successful separation of BSPMNPs, a magneto-CE system was developed and successfully demonstrated for magnetic trapping of BSPMNPs

using 10 mM sodium phosphate (pH 7.8) as electrolyte. The magnetic capture of BSPMNPs electrically driven at constant voltage of 15 kV and pressure driven at 40 mbar in a fused silica capillary of 60 cm total length and 75 µm id has shown that when 4 square NdFeB magnets are sequentially positioned within a capillary zone, and BSPMNPs flow by pressure, ca 68% of them are captured, corresponding to 20% higher capture than electrically driven BSPMNPs. A single layer magnetic coil (4 to 43 cm) of copper wire winding around a fused silica capillary was made but proven to be ineffective for BSPMNPs capture. Therefore, in the future, it is expected to develop a magnetic coil with several loops of copper wire around a fused silica capillary and a core made of iron to concentrate and amplify the magnetic field. The results obtained for the magneto CE-system can be useful for further design of magnetic fields (permanent magnets or electromagnets) for more effective nanoparticle's capture.

Highly charged electrostatic interactions between nanoparticles and cells have been demonstrated to induce membrane adsorption and intracellular uptake. In this dissertation, interactions between MNP-COOH (ca. 10 nm) and *E. coli* TOP10 were induced by ITP and analysed as a labelling method. This labelling method has the advantages of being applied in a very simple way and is rapid and applicable for every kind of cell. The presence of colonies was indicative of MNP-COOH incorporation or attachment to the *E. coli* TOP10 cells surface during ITP focusing, however, the sensitivity obtained was behind expectations. To increase the sensitivity, this method was applied to QD-COOH (10 nm diameter). The cells were subsequently recovered and visualised by fluorescence microscopy. The use of QD-COOH could save over 16 hours compared to the method for MNP-COOH by eliminating an overnight incubation step. Yet, no fluorescent cells were visualised, which can relate to their

small size and/or limited resolution of the fluorescence microscope used. To have a clear understanding of the capability and efficiency of ITP in cell uptake and interaction either with carboxylic acid functionalised MNPs and QDs more sensitive techniques for magnetic detection will be applied in further studies. For the analysis of MNP-COOH interaction and incorporation into E. coli a new detection setup will be used such as giant magnetoresistance (GMR), nuclear magnetic resonance (NMR) and superconducting quantum interference devices (SQUID), while for the analysis of carboxylic acid functionalised MNPs quantum dots, a more robust fluorescence microscope or flow cytometry will be used as an alternative. Given the issues associated to the sensitivity of E. coli TOP10 cells carrying MNPs and QDs after ITP, plasmid DNA molecules were then introduced into E. coli TOP10. A rapid ITP method for *E. coli* transformation that only required two electrolyte systems, application of constant voltage and low amounts of non-competent cells (10^5) and plasmid (0.1 µg) at room temperature was developed. This method provided high concentration of extracellular plasmid near the surface of each cell (ratio of 114,974:1 *vs.* 2:1 in CT and EP) improving the transformation rate up to 0.3% for pUC18 (about 1,000 higher than CT and EP) with survival rates greater than 60%. A range of plasmids up to 10 kb were successfully introduced into cells opening possibilities of using the developed method for the delivery of many other membrane impermeable solutes not only in bacteria but also in mammalian cells for screening of genes and drugs.

Jurkat cells are an immortalised line of human T lymphocyte cells that transfect poorly under electroporation, offering frequencies which are sometimes insufficient for their practical applications. The feasibility of using ITP to introduce plasmid DNA into Jurkat cells was demonstrated by injecting sequentially 0.19 µg of plasmid DNA

(pCMV6-AC-GFP) and $5x10^3$ Jurkat cells into a Rtx wax (fused silica) capillary with 60 cm total length and 100 µm ID and focused into 19 nL by ITP induced by application of constant voltage (3 kV). The expression of GFP was an indicator of transfection efficiency using 0.16 M sodium-phosphate (pH 7.3) as LE and 0.16 M sodium-HEPES (pH 7.3) as TE. In such electrolytes, the viability of Jurkat cells was above 80% for more than 10 hours. Jurkat cells were transfected at a rate of 88% with the vector pCMV6-AC-GFP, while EP of 10^6 and 10^3 cells only achieved 54% and 51%, respectively. The fact that both EP and ITP involves the physical interaction between an electric field and the cell membrane make them less dependent on cell type than other methods. However, ITP transfection is suitable for handling large sample sets when organized in 96-well plates adapted to a multichannel capillary electrophoresis device, which increases automation and sample processing throughput. This method appears as a supplement to the existing arsenal of methods for obtaining cellular expression of sequence information present on molecules of exogenous DNA without requiring complicated cell purification procedures and with no issues related to biosafety and mutagenesis as viral vectors do. The transfection success of ITP transfection encourages the application of this method as a newly emerging attractive option for recombinant protein production. The results obtained should encourage microbiologists and cell biologists to use CE to address questions related to their field.

In the future, the developed ITP methods will be implemented for the internalisation of plasmid DNA, nanoparticles, and other membrane-impermeable molecules in a portable CE system or microfluidic chip affordable for biological therapeutics. This technology may have commercial interest for numerous applications in different areas where gene delivery techniques are crucial, namely for vaccine development and

cancer immunotherapy, and delivery of fluorescent probes for cellular imaging. The configuration of the developed ITP methods into portable and microfluidic platforms will significantly reduce costs when compared to conventional techniques or operating a CE instrument, while increasing simplicity of use.